

Supporting information

Dynamic adjustment of emission from both singlets and triplets: the role of excited state conformation relaxation and charge transfer in phenothiazine derivatives

Weidong Qiu,^a Xinyi Cai,^a Mengke Li,^a Liangying Wang,^a Yanmei He,^a Wentao Xie,^a Zijian Chen,^a Ming Liu^a and Shi-Jian Su^{*a,b}

^aState Key Laboratory of Luminescent Materials and Devices and Institute of Polymer Optoelectronic Materials and Devices, South China University of Technology, Guangzhou 510640, China.

^bSouth China Institute of Collaborative Innovation, Dongguan 523808, China.

E-mail: mssjsu@scut.edu.cn

Table of contents

1. Experimental Procedures
2. Results and discussion
 - 2.1 Computation
 - 2.2 Photophysical properties
 - 2.3 Single crystal analysis
 - 2.4 Device fabrication and characterization
3. Synthesis Routes
4. Reference

1. Experimental procedures

Chemical structure characterization. ^1H and ^{13}C NMR spectra were measured on Bruker NMR spectrometer operating at 600 and 150 MHz, respectively. The samples were dissolved in deuterated chloroform (CDCl_3) and measured at ambient temperature. Atmosphere pressure chemical ionization (APCI) mass spectra were obtained using a JEOL JMS-K9 mass spectrometer. Small molecule single crystal X-ray analysis was conducted on Rigaku XtaLAB P2000 FR-X with a rotating copper anode and a Pilatus 200K detector at room temperature. Powder XRD was conducted on a polycrystal X-ray diffraction (Rigaku SmartLab SE). Cyclic voltammetry (CV) measurement was conducted using the CHI-600D electrochemical workstation (with glassy carbon electrode as working surface, a platinum wire as counter electrode and Ag/AgCl as reference electrode) scanning at the rate of 50 mV/s in nitrogen-saturated 0.1 mol/L $n\text{-Bu}_4\text{NPF}_6$ anhydrous solution.

Photophysical characterization. UV-vis absorption spectra were recorded using Perkin-Elmer Lambda 950-PKA instrument. Fluorescence and phosphorescence spectrum were recorded by a FluoroMax-4 spectrofluorometer. Transient PL decay spectrum and temperature dependent PL spectrum of films and single crystal were conducted on FL980 (Edinburgh Instrument) where the lifetimes in 50 μs time range were measured with a TCSPC laser and the lifetimes in ms and s time range were measured with a micro second flash lamp and Xeon lamp, respectively. Photoluminescent quantum yields (PLQYs) were measured utilizing an integrating sphere of Hamamatsu absolute PL quantum yield spectrometer (Hamamatsu, C11347-01).

Quantum chemical calculation. The calculations were performed using the Gaussian 09 E01 package.¹ The ground state, excited state geometries and flexible potential surface scanning were optimized in M062x/TZVP level in gas phase and according to density functional theory (DFT) and time dependence density functional theory (TD-DFT).²⁻⁵ For triplet geometries, unrestricted DFT (UDFT) was adopted to optimize triplet geometries. Dimer structures were extracted from single crystal XRD results and dimers with π - π interactions were selected. Before calculation, restricted geometry optimization was conducted in B3LYP/6-31G* level by “freezing” all atoms except for hydrogen and the transition character and energy were further calculated in M062x/TZVP level. The natural transition orbitals (NTOs) were analyzed using Multiwfn and visualized with VMD software.^{6,7} The SOC matrix were calculated with PySOC.⁸

2. Results and Discussion

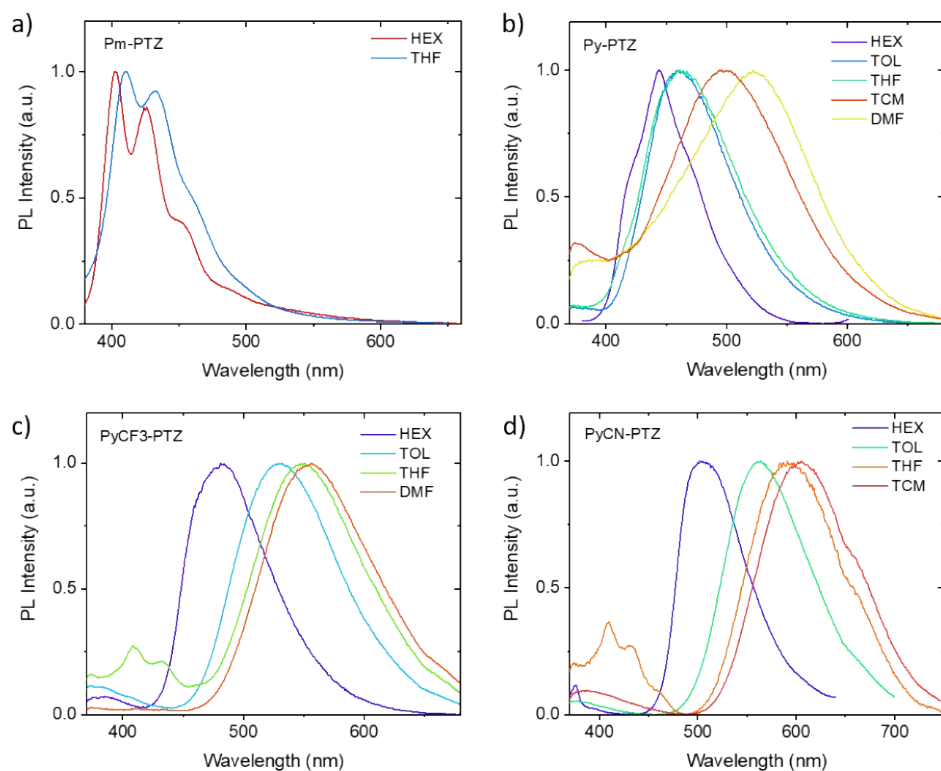


Fig. S1. Solvatochromism effect of these compounds in different solvents (concentration: 10^{-4} M) including hexane (HEX), toluene (TOL), tetrahydrofuran (THF), trichloroethane (TCM) and N, N-Dimethylformamide (DMF). Pm-PTZ exhibits little redshift in THF, which indicates a LE feature and Py-PTZ has a hybrid local and charge transfer character. In the CT compounds, the largest redshift is noted for PyCN-PTZ, indicating the largest ICT strength and large excited state geometry reorganization. In solvent with large polarity, dual emissions from planar (short wavelength) and twist conformation (long wavelength) were observed.

Table S1. DFT, TD-DFT and UDFT optimized geometry parameters including bending angles of phenothiazine (α), twisting angles (β) and bond lengths (l) between donor and acceptor, simulated HOMO and LUMO energy level and dipole moments (D) of all molecules. (Based on M062X/TZVP in gas phase).

Molecules	S_0 geometry					S_1 geometry					T_1 geometry				
	α	β	l	HOMO/LUMO	D	α	β	l	HOMO/LUMO	D	α	β	l	HOMO/LUMO	D
	[°]	[°]	[Å]	[eV]	[Debye]	[°]	[°]	[Å]	[eV]	[Debye]	[°]	[°]	[Å]	[eV]	[Debye]
Pm-PTZ	37.63	4.92	1.40	-5.48/-0.97	1.97	0.04	89.99	1.49	-5.66/-1.56	5.86	0.00	89.99	1.45	-5.65/-1.18	5.29
						35.28	5.62	1.37	-6.91/-0.51	2.18					
Py-PTZ	37.01	20.44	1.40	-5.31/-0.56	1.86	13.28	87.77	1.44	-5.77/-0.66	4.16	8.87	88.31	1.44	-5.68/-0.58	4.27
PyCF3-PTZ	37.59	18.05	1.39	-5.65/-0.95	3.95	9.76	87.78	1.44	-6.10/-1.55	1.67	7.03	89.66	1.44	-5.97/-1.27	1.63
PyCN-PTZ	37.53	17.51	1.39	-5.79/-1.34	5.77	7.47	87.96	1.44	-6.14/-1.81	2.26	8.39	89.70	1.44	-6.12/-1.74	2.17

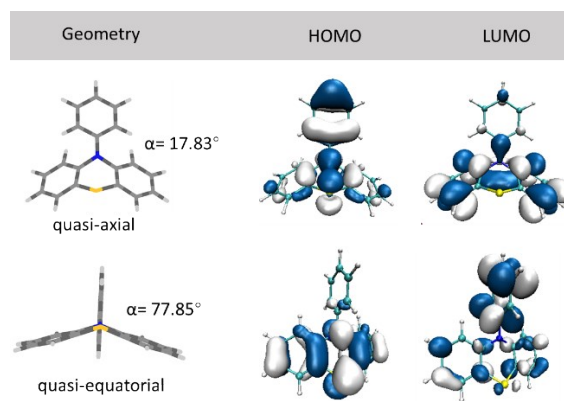


Fig. S2. Optimized ground state geometries and frontier orbitals of PTZ-Ph.

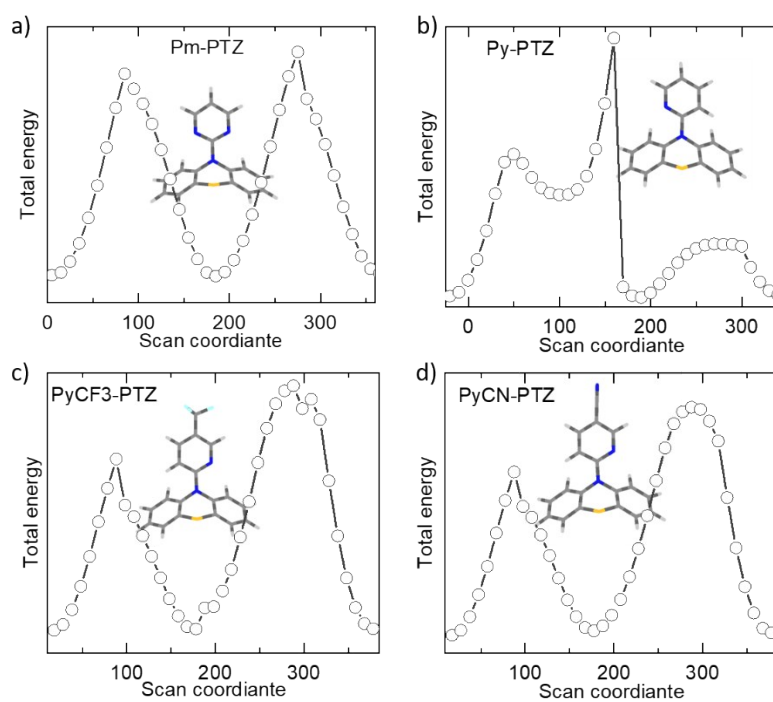


Fig. S3. Flexible potential surface scanning on the energy of ground state geometries of the four molecules.

Table S2. Summary of hole and particle distributions, corresponding eigenvalues, transition energy and oscillator strengths of Pm-PTZ monomer.

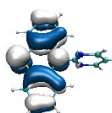
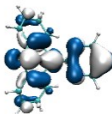
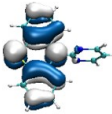
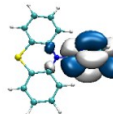
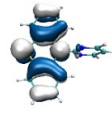
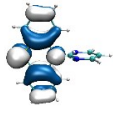
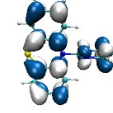
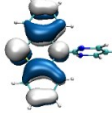
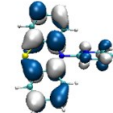
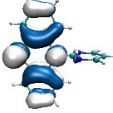
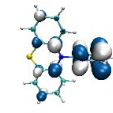
	Pm-PTZ					
	S ₀ geometry		S ₁ geometry		T ₁ geometry	
	Hole	Particle	Hole	Particle	Hole	particle
S ₁						
	98.76%	4.38 eV f=0.0020	99.95%	2.35 eV f= 0.0001		
S ₂						
	98.20%	4.53 eV f=0.0093	99.90%	3.28 eV f= 0.0000		
T ₁						
			99.24%	2.75 eV f=0.0000	96.73%	2.41 eV f=0.0000
T ₂						
			95.30%	3.27 eV f=0.0000	98.50%	2.81 eV f=0.0000

Table S3. Summary of hole and particle distributions, corresponding eigenvalues, transition energies and oscillator strengths of Py-PTZ monomer.

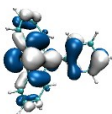
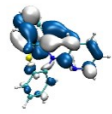
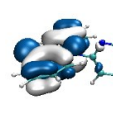
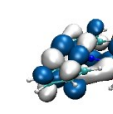
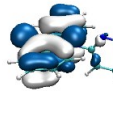
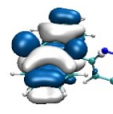
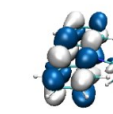
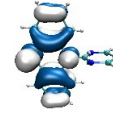
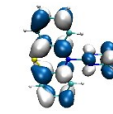
	Py-PTZ					
	S ₀ geometry		S ₁ geometry		T ₁ geometry	
	Hole	Particle	Hole	Particle	Hole	particle
S ₁						
	93.28%	4.49 eV f=0.0393	99.38%	2.97 eV f= 0.0000		
S ₂						
			97.94%	3.47 eV f= 0.0064		
T ₁						
			95.97%	2.48 eV f=0.0000	96.74%	2.41 eV f=0.0000

Table S4. Summary of hole and particle distributions, corresponding eigenvalues, transition energies and oscillator strengths of PyCF3-PTZ monomer.

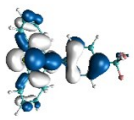
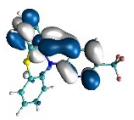
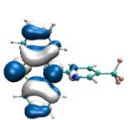
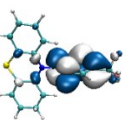
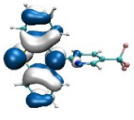
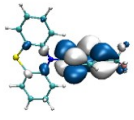
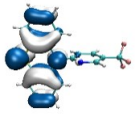
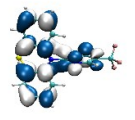
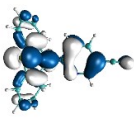
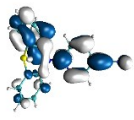
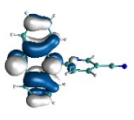
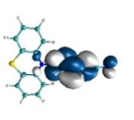
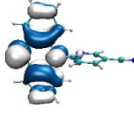
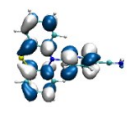
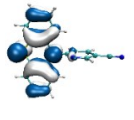
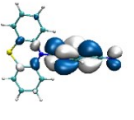
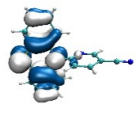
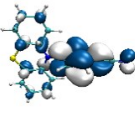
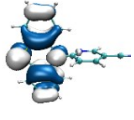
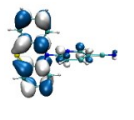
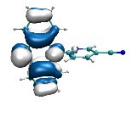
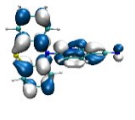
PyCF3-PTZ							
		S ₀ geometry		S ₁ geometry		T ₁ geometry	
		Hole	Particle	Hole	Particle	Hole	Particle
S ₁							
		90.53%	4.57 eV f=0.0076	99.81%	2.58 eV f= 0.0001		
T ₁							
				98.51%	2.53 eV f= 0.0000	98.56%	2.43 eV f=0.0000

Table S5. Summary of hole and particle distributions, corresponding eigenvalues, transition energies and oscillator strengths of PyCN-PTZ monomer.

PyCN-PTZ							
		S ₀ geometry		S ₁ geometry		T ₁ geometry	
		Hole	Particle	Hole	Particle	Hole	particle
S ₁							
		95.95%	4.48 eV f=0.4734	99.89%	2.43eV f= 0.0000		
S ₂							
				99.29%	3.33 eV f= 0.0001		
T ₁							
				99.53%	2.41 eV f=0.0000	98.56%	2.41 eV f=0.0000
T ₂							
				94.65%	2.82 eV f=0.0000	94.74%	2.83 eV f=0.0000

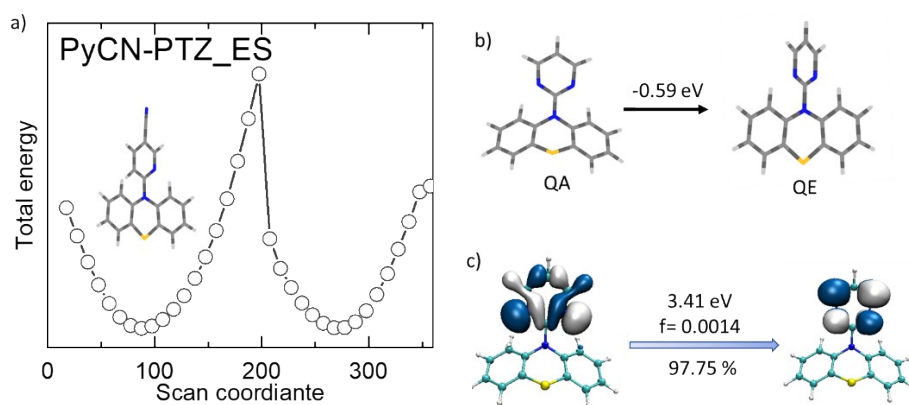


Fig. S4. a) Flexible potential surface scanning of PyCN-PTZ on the energy of S_1 geometry in B3LYP-D3/TZVP level (B3LYP with Grimme's DFT-D3 correction) which indicates that there is only one stable twist conformation in excited state. b) Excited state (S_1) geometry of Pm-PTZ. Dual conformations are noted in the excited state of Pm-PTZ with quasi-equatorial one has lower energy. c) NTO of S_1 state in quasi-axial conformation of Pm-PTZ.

Table S6. Experimental (in hexane) and calculated photophysical properties of the four compounds in monomeric state.

Molecules	$\lambda_{\text{Absorption}}$		$\lambda_{\text{Emission}(S_1)}$		$\lambda_{\text{Emission}(T_1)}$		Stoke shift (nm)
	Exp. (nm)	Calc. (nm)	Exp. (nm) ^{a)}	Calc. (nm)	Exp.(nm)	Calc.(nm)	
Pm-PTZ	304	283	402 (364)	492	401	515	98
Py-PTZ	305	276	443 (367)	417	434	515	138
PyCF3-PTZ	307	271	482 (365)	481	414	510	175
PyCN-PTZ	315	276	505 (393)	510	459	514	190

^{a)} Peak wavelength of PL spectra measured at 77K.

Table S7. Photophysical properties of the four compounds in film state.

Molecules	$S_1^{\text{a)}$	$T_1^{\text{a)}$	ΔE_{ST}	PLQY ^{b)}	$\tau_{\text{prompt}}^{\text{c)}$	$k_{\text{fluor.}}^{\text{d)}$	$\tau_{\text{delay}}^{\text{c)}$	$\Phi_{\text{prompt}}/$ $\Phi_{\text{delay}}^{\text{c)}$
	[eV]	[eV]	[eV]	[%]	[ns]	[10^8 s^{-1}]	[μs]	
Pm-PTZ	3.00 ^{e)} /3.42 ^{d)}	2.89 ^{e)} /2.46 ^{h)}	/	2.98	2.61	-	417.93 ⁱ⁾ / 16650 ^{j)}	-
Py-PTZ	2.77	2.47	0.30	0.22	-	-	14.19	-
PyCF3-PTZ	3.06	2.88	0.18	16.31	4.76	9.16	55.26	26.74/73.26
PyCN-PTZ	2.75	2.63	0.12	18.02	9.01	5.59	24.82	27.93/72.06

^{a)} For CT type emission profile, the energy was calculated from the onset of emission while for LE type emission, the energy is calculated according to the peak wavelength. ^{b)} Measured in air. Because of the triplet quenching of oxygen, large conformation relaxation and n- π^* transition character in the excited state, the PLQY is low compared with common fluorescence or TADF materials. ^{c)} The lifetime and percentage of prompt and delay component was fitted according to exponential decay relation. ^{d)} fluorescence rate constant $k_{\text{fluor.}} = \text{PLQY} * \Phi_{\text{prompt}} / \tau_{\text{prompt}}$ ^{e), f)} Obtained from the peak of planar and twist conformation in PL spectrum respectively. ^{g), h)} Calculated from the onset and peak intensity of phosphorescence spectrum at 77K and 298K respectively. ^{i), j)} Measured at 460 nm and 550 nm respectively.

Table S8. Photophysical properties of the four compounds in powder state.

Molecules	$S_1^{\text{a)}$	$T_1^{\text{a)}$	ΔE_{ST}	PLQY	$\tau_{\text{prompt}}^{\text{b)}$	τ_{delay}	$\Phi_{\text{phos}}^{\text{b)}$
	[eV]	[eV]	[eV]	[%]	[ns]	[ms]	[%]
Pm-PTZ	2.90	2.24	0.66	6.21	1.60	15.37	5.63
Py-PTZ	2.91	2.41	0.50	8.06	2.91	38.58	7.70
PyCF3-PTZ	3.15	2.47	0.68	7.54	1.48	18.09	4.18
PyCN-PTZ	2.88	2.34	0.54	22.05	3.98	11.82	12.81

^{a)} Calculated according to the peak wavelength. ^{b)} Calculated according to the area of the steady state PL spectrum and PLQY of powders.

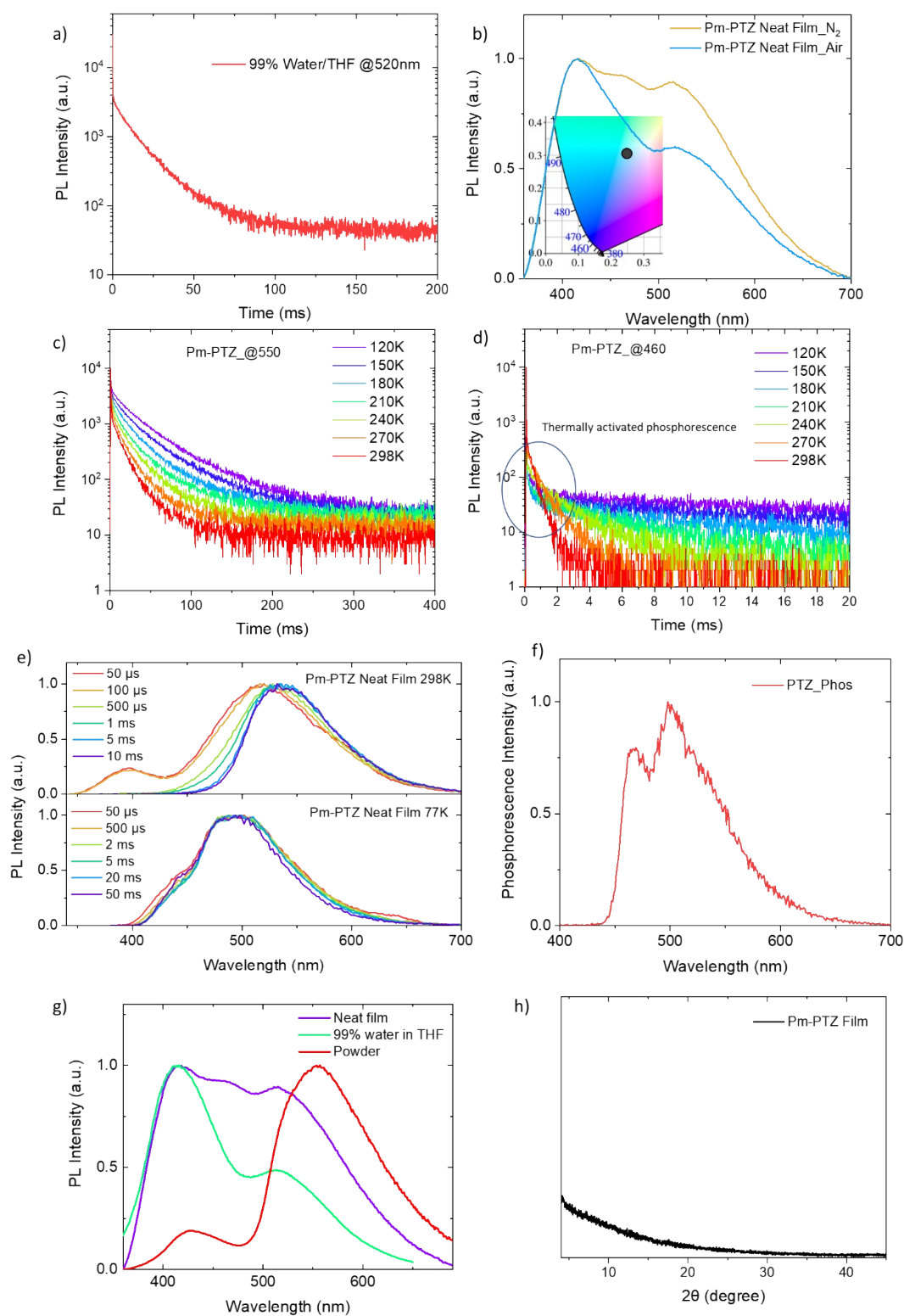


Fig. S5. a) Transient PL spectra of Pm-PTZ in THF/H₂O (v/v, 1:99, 10⁻⁴ M) mixed solvent measured at 520 nm, which indicates that the long lifetime phosphorescence at 520 nm is originated from molecular aggregates. b) PL spectra of Pm-PTZ neat film in air and under N₂ atmosphere, and the insert graph denotes the calculated CIE coordinate (0.25, 0.31) according to the spectra under N₂ atmosphere, which is a cold white emission. Temperature dependence transient PL spectra of Pm-

PTZ neat film measured at c) 550 nm and d) 460 nm. e) Gated phosphorescence spectra of Pm-PTZ neat film at RT and 77K. f) Phosphorescence spectrum of PTZ monomer in toluene solution measured at 77K. g) Comparison of PL spectra of Pm-PTZ neat film, aggregates in 99% water/THF solution and powder. h) X-ray diffraction pattern of Pm-PTZ neat film on a silicon substrate

A thermally activated region was observed at lifetime < 2 ms region from transient PL at 460 nm, indicating the emission comes from another excited state. In combined with the redshift emission with increasing delay lifetime and similar phosphorescence spectrum of PTZ monomer in toluene, we attributed this emission to phosphorescence of PTZ moiety. TD-DFT calculation results listed in Table S2 also indicates that NTO of T_2 transition in S_1 conformation or T_1 transition in T_1 conformation mainly distributes on PTZ moiety with $n-\pi^*$ transition character. Thus, it is reasonable to deduce that the emission at 460 nm with shorter lifetime is originated from the PTZ moiety.

The phosphorescence spectra of aggregates in film state and 99% water/THF solution is blue shift in comparison with that in powder (micro crystal). And XRD of film indicates that the film was in amorphous state. These results indicate that the formation of ordered molecular packing structure is not the necessary condition for long wavelength pure organic phosphorescence. And RTP in long wavelength can be realized by forming triplet excimer by in $\pi-\pi$ interaction in amorphous film.⁹

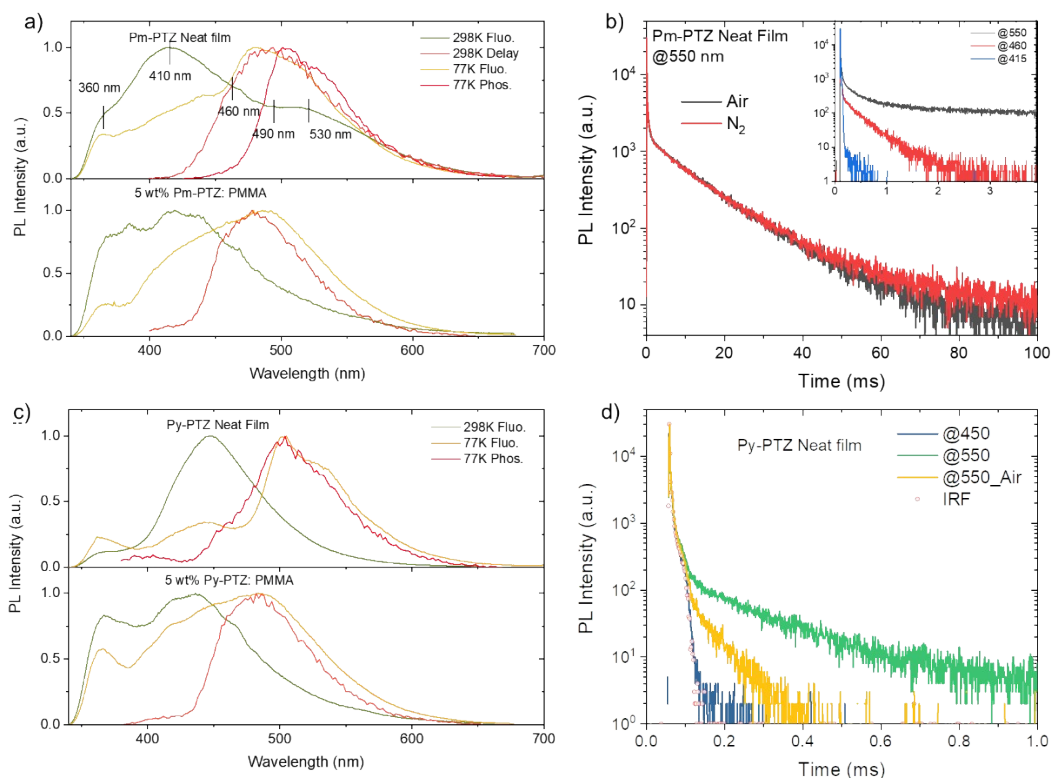


Fig. S6. Fluorescence and phosphorescence spectra at 298K and 77K for neat film and 5 wt% PMMA doped film of a) Pm-PTZ and c) Py-PTZ. Transient PL spectra of b) Pm-PTZ, d) Py-PTZ neat film measured at different wavelength.

The multiple emission peaks of Pm-PTZ was marked by black bars at the corresponding wavelength. According to temperature dependence PL at 360 nm, PL of 5 wt% PMMA doped film and TD-DFT calculation results, 360 nm emission belongs to the higher energy planar conformation of Pm-PTZ while the fluorescence peaking at 410 nm is normal fluorescence of the twist conformation. The thermally activated phosphorescence emission at 460 nm belongs to PTZ moiety. And the phosphorescence of Pm-PTZ monomer peaks at 490 nm, which was confirmed by the phosphorescence spectrum of neat film at RT and 5 wt% PMMA doped film at 77K. And the long wavelength phosphorescence at 530 nm is from molecular aggregates. Multiple emission behaviors of Py-PTZ was also observed, however, the PLQY and lifetime is lower and shorter than its powder sample, which is probably due to the poor intermolecular interaction in film state to “protect” triplet excitons from quenching and non-radiative transition in amorphous film.

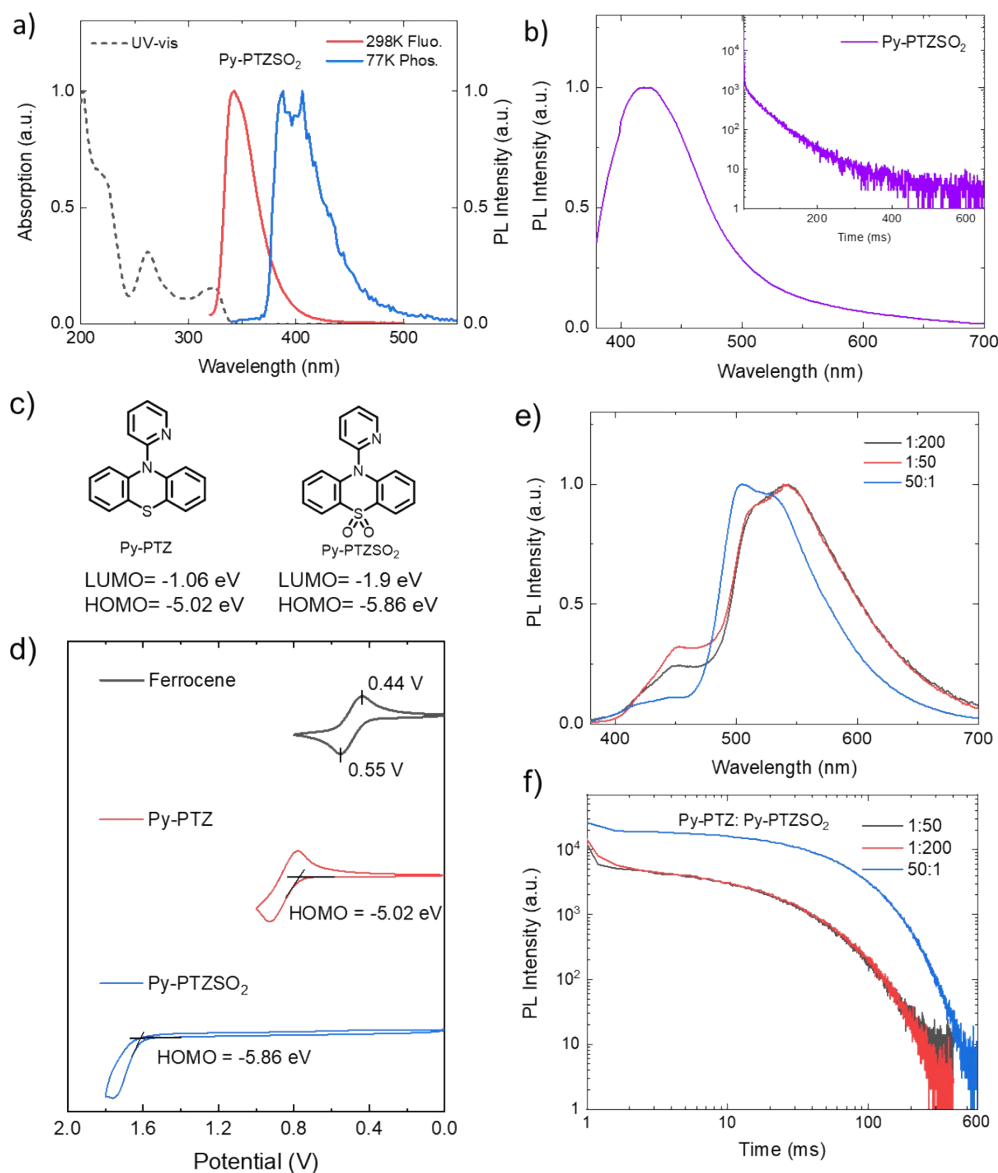


Fig. S7. a) Absorption, fluorescence and phosphorescence spectra of Py-PTZSO₂ in hexane solution (10⁻⁴ M). b) PL and transient PL spectra of Py-PTZSO₂ crystal. c) Molecular structures and HOMO, LUMO energies of Py-PTZ and Py-PTZSO₂. The HOMO energy is obtained by cyclic voltammetry measurement while LUMO energy is calculated according to the HOMO energy and the onset of absorption spectrum. d) CV of Py-PTZ and Py-PTZSO₂. PL e) and transient PL f) spectra of the Py-PTZ: Py-PTZSO₂ doping systems (mass ratio: 1:200, 1:50, 50:1).

The overlapped PL and transient PL spectra of the mixed system indicates that the doping of Py-PTZSO₂ with deeper HOMO and LUMO energy in Py-PTZ system has little influence on the phosphorescence emission. And the decay of phosphorescence follows an exponential law, which is different from organic long persistence luminescence system following a power law decay.^{10, 11} Moreover, using Py-PTZSO₂ as “host”, the doped system exhibits the same phosphorescence lifetime as Py-PTZSO₂. This result indicates that the formation of “heterojunction” in organic system is not sufficient for organic long persistence luminescence and more mechanism study is

needed.

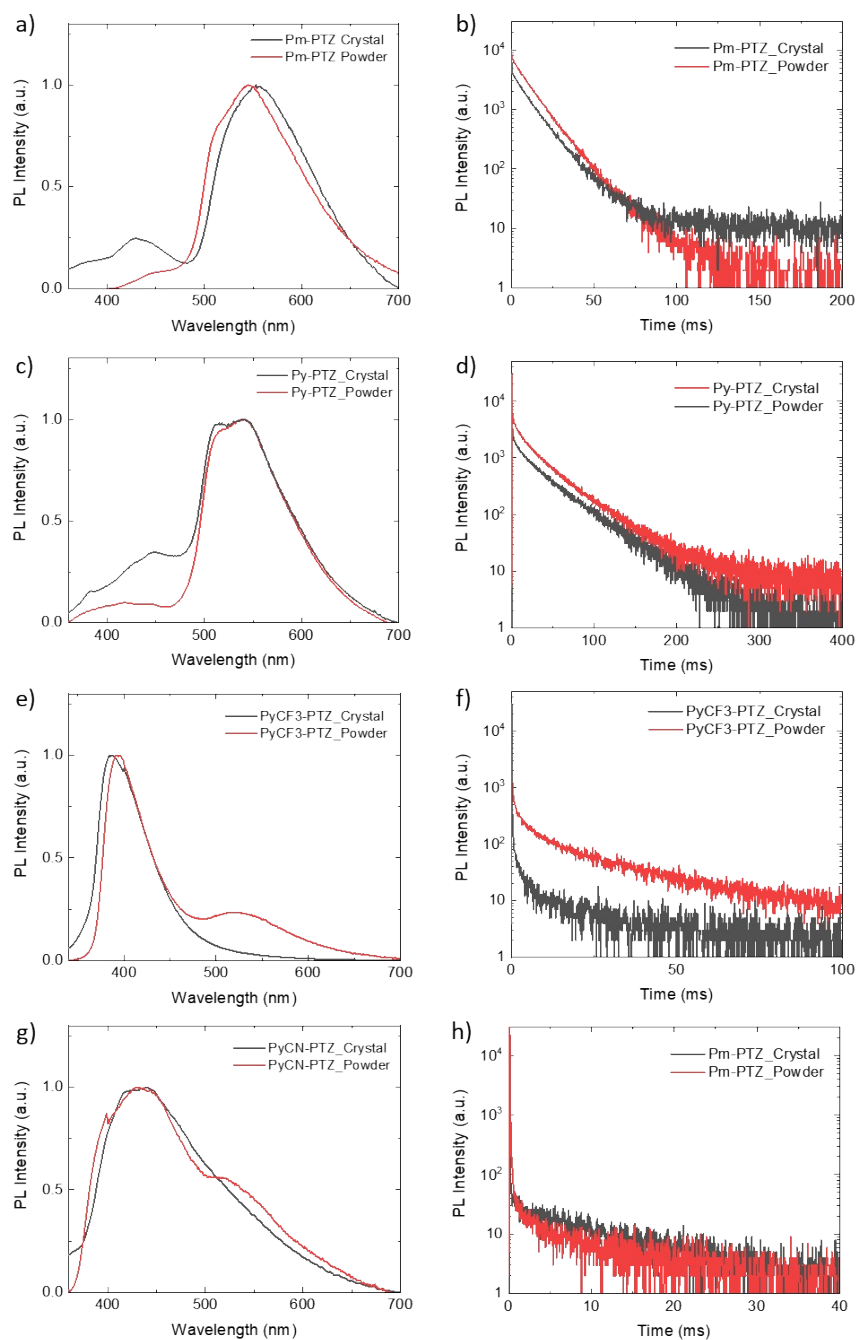


Fig. S8. Steady state PL spectra and transient PL spectra of a), b) Pm-PTZ, c), d) Py-PTZ, e), f) PyCF3-PTZ and g), h) PyCN-PTZ single crystal and powder samples.

The crystalline powder and single crystal samples show similar emission peak wavelength and phosphorescence lifetime. However, there is difference in relative intensity of fluorescence and phosphorescence peaks, and single crystal samples have less phosphorescence component. This might be due to a portion of molecules can change their planar conformation to the twisted one to accelerate intersystem crossing in powder sample, which is in accordance to the conclusion of this manuscript.

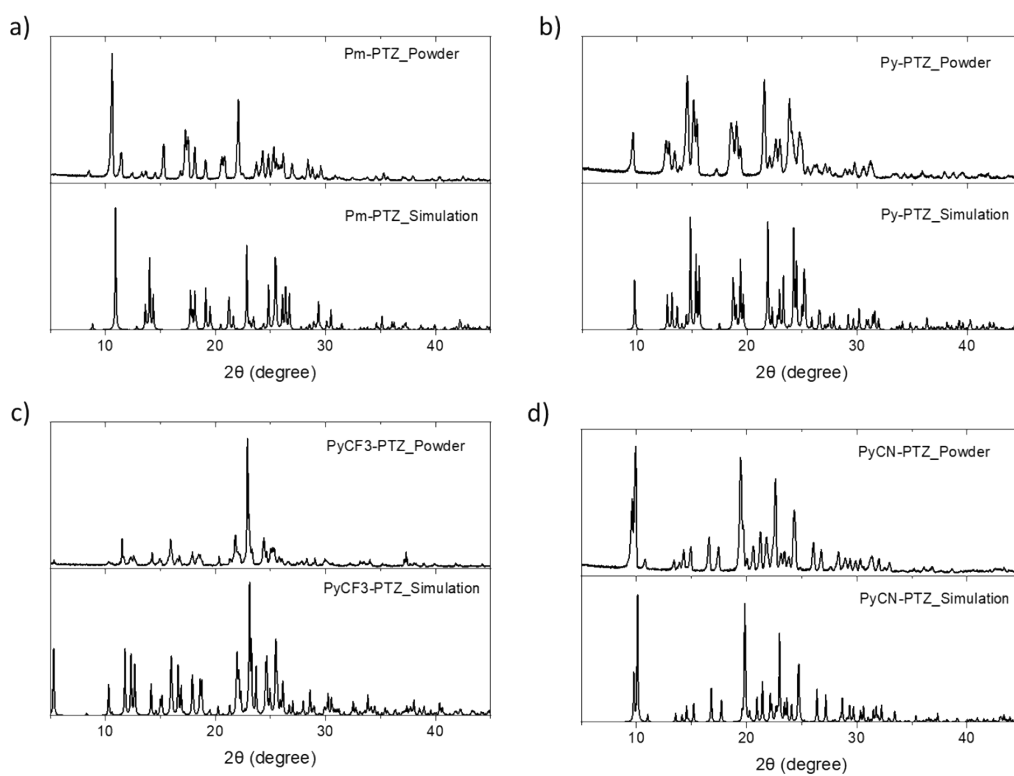


Fig. S9. Measured and simulated powder X-ray diffraction patterns for powders of a) Pm-PTZ, b) Py-PTZ, c) PyCF3-PTZ and d) PyCN-PTZ.

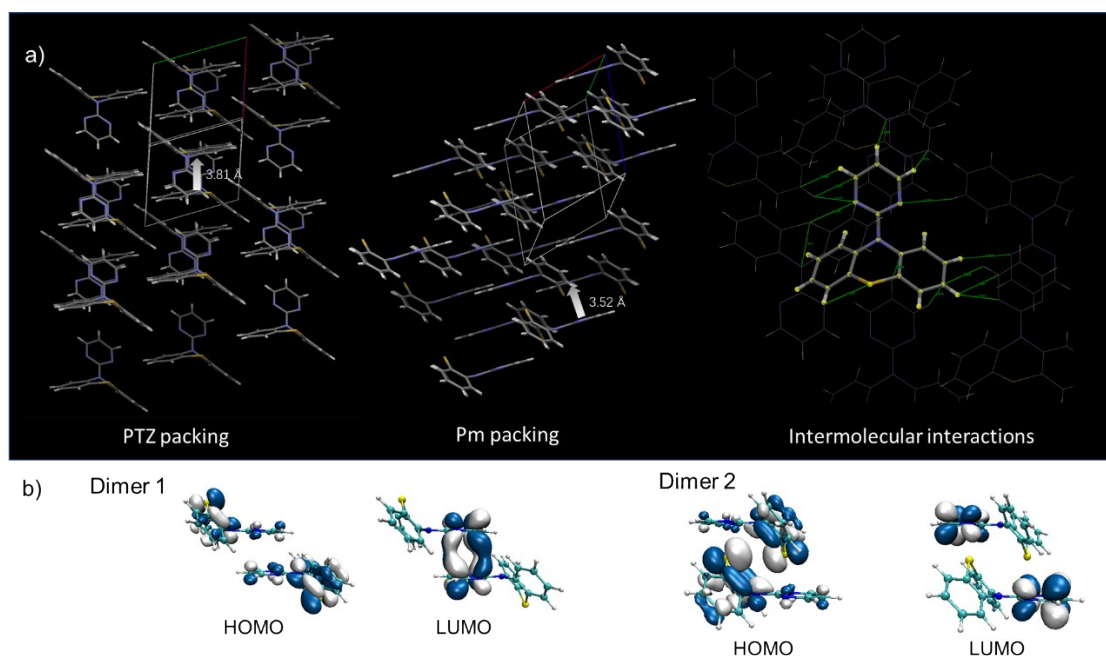


Fig. S10. a) Single crystal packing and intermolecular interactions of Pm-PTZ, where ten CH \cdots π interactions, five CH \cdots N interactions and two N \cdots S interactions were noted. b) HOMO and LUMO orbitals (isovalue: 0.03) of two dimers with close π - π interactions form single crystal structure.

The overlap of HOMO of dimer 1 was noted, indicating the existence of strong π - π interactions (distance: 3.52 Å). And the dimer formation in crystal state will reduce the triplet state energy, forming a “stabilized triplet state”. Moreover, according to the Marcus theory, the triplet transportation can be regarded as simultaneous migration of an electron and a hole, which depends on the overlap of HOMO and LUMO orbitals.¹² And the limited overlap of HOMO would reduce the triplet migration and reduce the quenching of triplet excitons by triplet-triplet annihilation.^{13, 14}

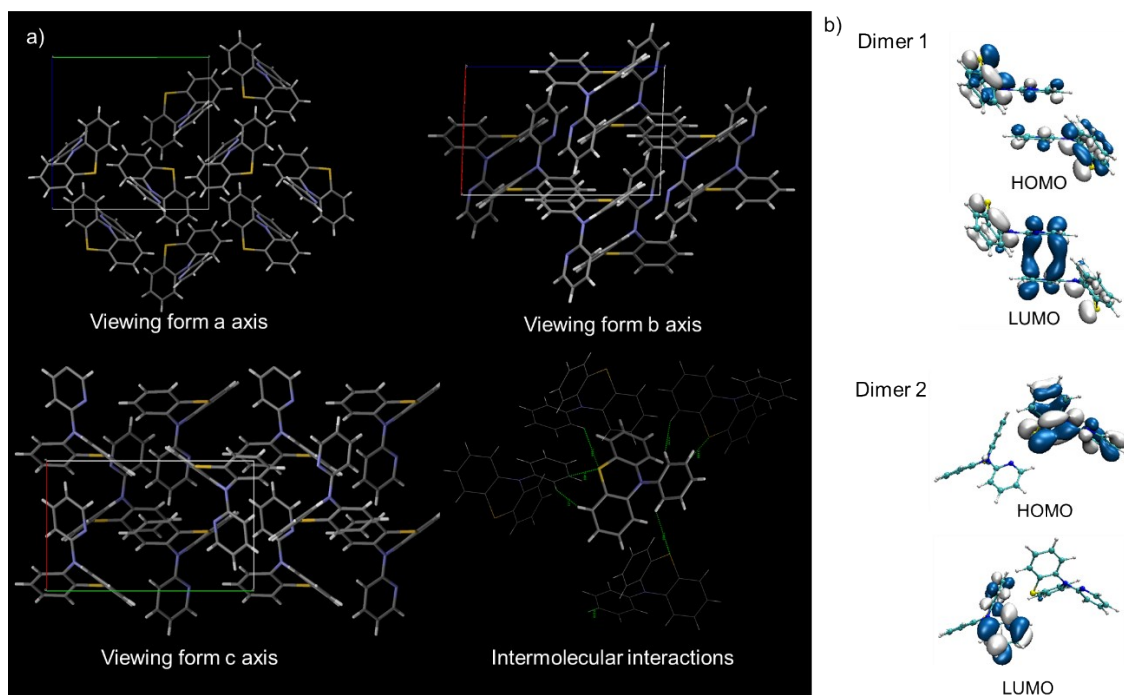


Fig. S11. a) Single crystal packing and intermolecular interactions of Py-PTZ. Two S \cdots H hydrogen bonds, two S \cdots π interactions and two CH \cdots CH interactions were noted. b) HOMO and LUMO orbitals of two dimers from single crystal structure.

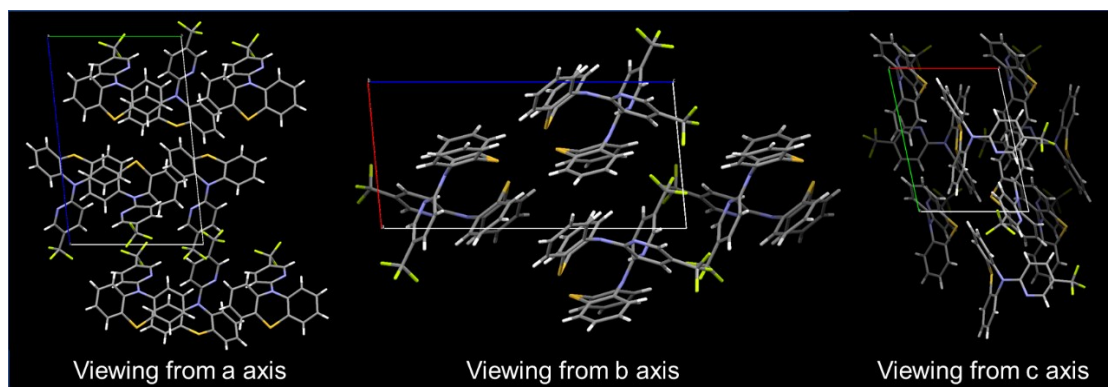


Fig. S12. Single crystal packing of PyCF3-PTZ.

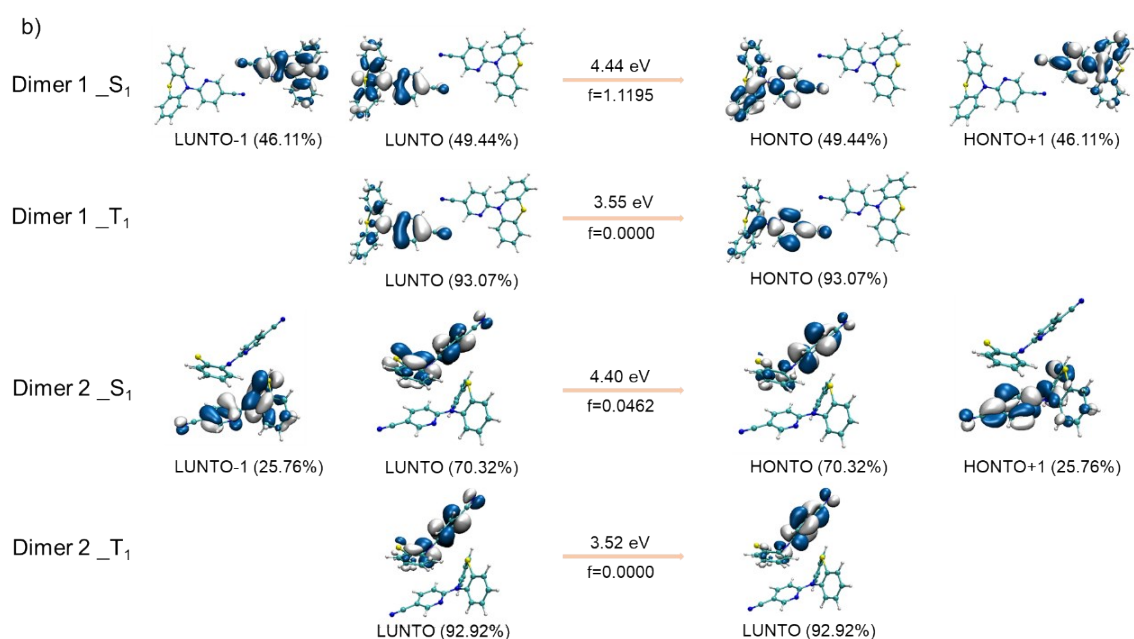
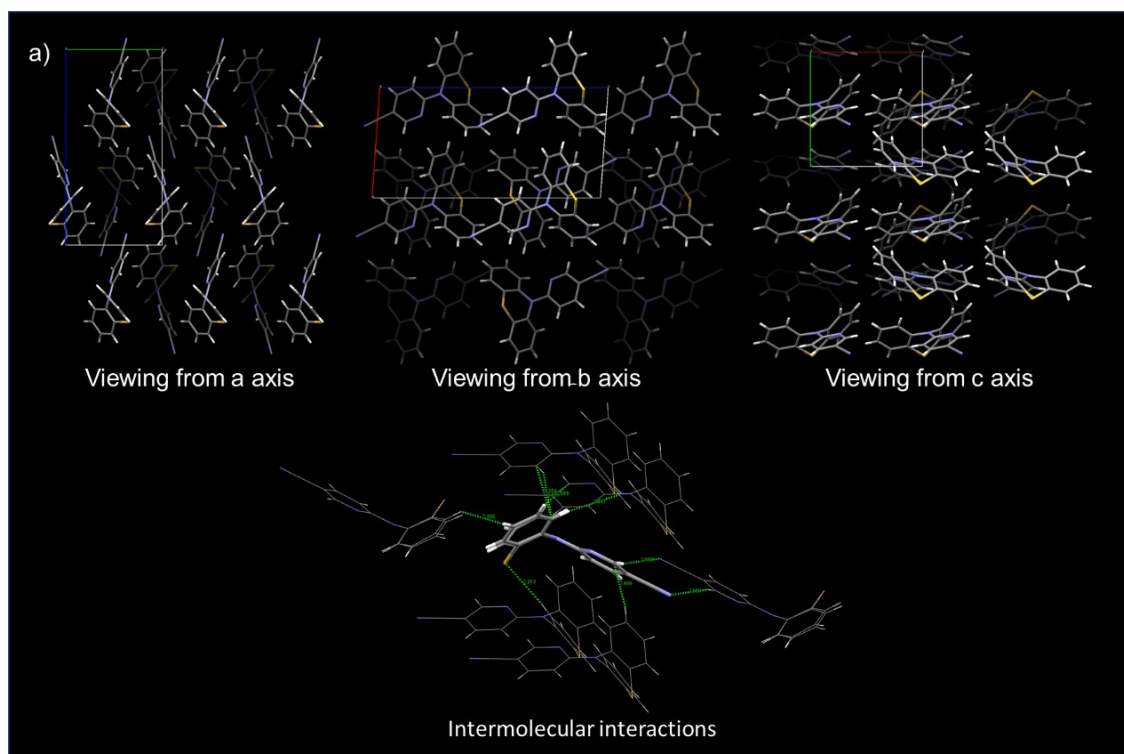


Fig. S13. a) Single crystal packing of PyCN-PTZ single crystal. Six $\text{CH}\cdots\pi$ interactions, two $\text{N}\cdots\text{CH}$ hydrogen bonds and one $\text{CH}\cdots\text{S}$ hydrogen bond are noted for one molecule. b) NTOs of singlet and triplet state of two dimers extracted from single crystal structure. Because of the symmetry of structures from single crystal, S_1 , S_2 and T_1 , T_2 are degenerate states in dimer 1 and only NTOs of S_1 and T_1 were given. The NTO pairs mainly distribute on single molecular without dispersion distribution and there is little difference of vertical excitation energy between the dimer and monomer, indicating less electron coupling in single crystal of PyCN-PTZ, and single crystal only serves as a rigid matrix for independent emission of monomer.

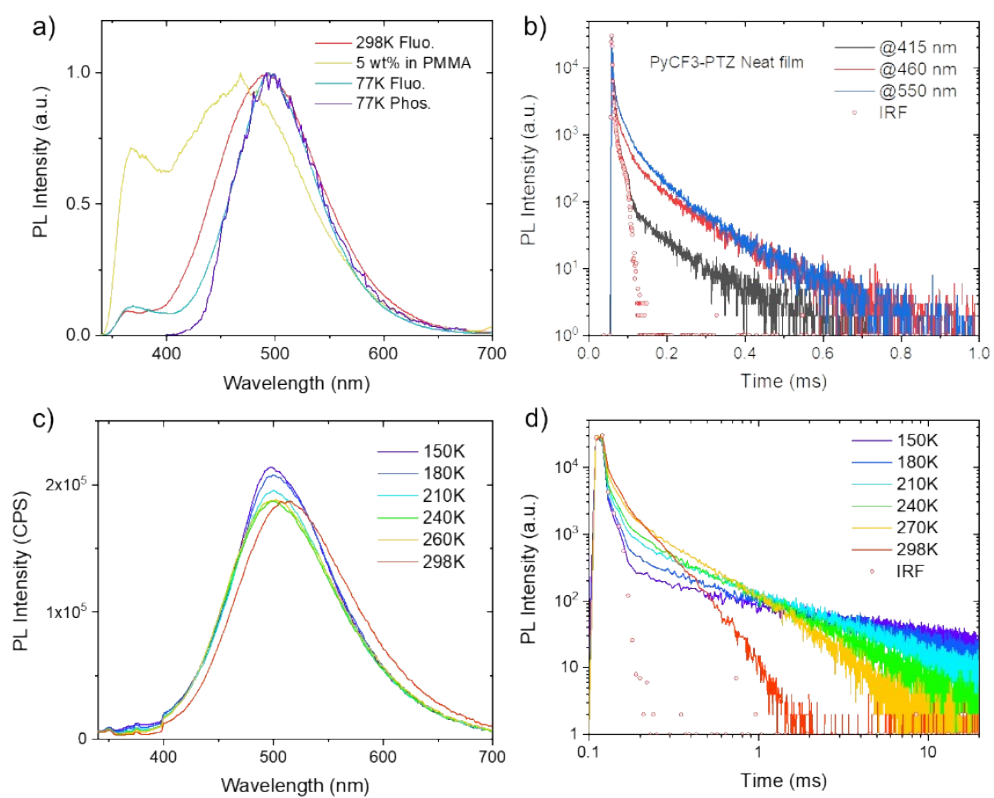


Fig. S14. a) Steady state PL (measured at 298K and 77K) and phosphorescence spectra of PyCF3-PTZ neat film and PL of 5 wt% doped film in PMMA. b) transient PL spectra of PyCF3-PTZ neat film at different wavelength under N₂ atmosphere. c) Temperature dependence PL and d) transient PL spectra of PyCF3-PTZ neat film.

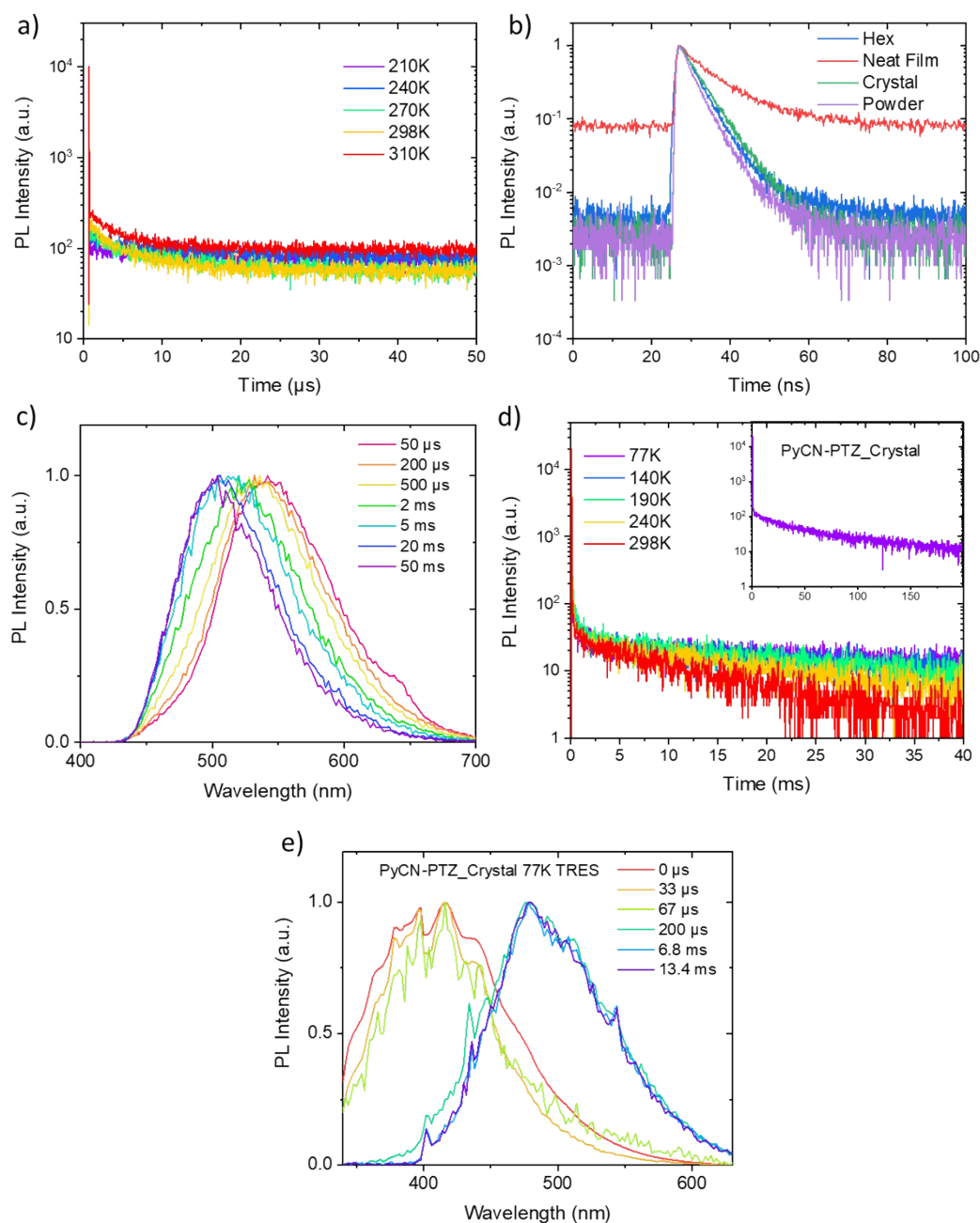


Fig. S15. a) Temperature-dependence transient PL spectra of PyCN-PTZ neat film in 50 μs time range. Note that the delay component involving triplet excitons are highly depends on the excitation density. Due to lower frequency of the TCSPC laser in 50 μs mode, the delay component is less than that in ms or ns range. And only small percentage of thermally activated region at <5 μs was observed at high temperature, indicating that the emission is dominated by fluorescence and phosphorescence at RT. b) Transient PL spectra in 100 ns range of PyCN-PTZ in hexane, neat film, single crystal and powder states. c) Phosphorescence spectra of PyCN-PTZ neat film at 77K with different delay time. d) Temperature-dependence transient PL spectra of PyCN-PTZ single crystal measured at 500 nm. f) Time resolve emission spectra (TRES) of PyCN-PTZ single crystal. The emission peaking at 490 nm at lifetime > 60 μs (lifetime of the microsecond flash lamp: ~ 50 μs) region is delay component which originates from phosphorescence of PyCN-PTZ single crystal

(planar conformation of PyCN-PTZ).

A prolonged prompt emission lifetime and reduced prompt component of PyCN-PTZ film is noted in Fig. S15b in compared with fluorescence in solution and solid stated. In hexane with low polarity, the TICT process does not dampen the fluorescence emission because of the less extent of ICT and fast conformation relaxation (usually a few ps in solution¹⁵). And the prompt lifetime is close to that in powder and single crystal with planar conformation. For aromatic amine containing structures, the typical rate constant of ISC is about 10^8 S^{-1} .¹⁶ In the neat film of PyCN-PTZ, due to the TICT process, the rate constant of ISC become competitive with the slowed radiative transition, which populates the triplet state. Moreover, the rate constant of thermally activated delayed fluorescence is a few orders of magnitude lower than radiative transition. Thus, in combined with large spin orbital coupling in the transition forbidden TICT state, phosphorescence emission outweighs the emission of TADF in PyCN-PTZ neat film.

The gradually redshift emission indicates the conformation distribution in neat film at 77K and the planar conformation (emissions at 490 nm) has longer phosphorescence lifetime than the twist one (emissions at 550 nm) which results from the strong spin mixing in twist conformation. Thus, the conformation-relationship could be revealed where the planar conformation has a long triplet lifetime and lower intensity while the twist one has high intensity but shorter lifetime.

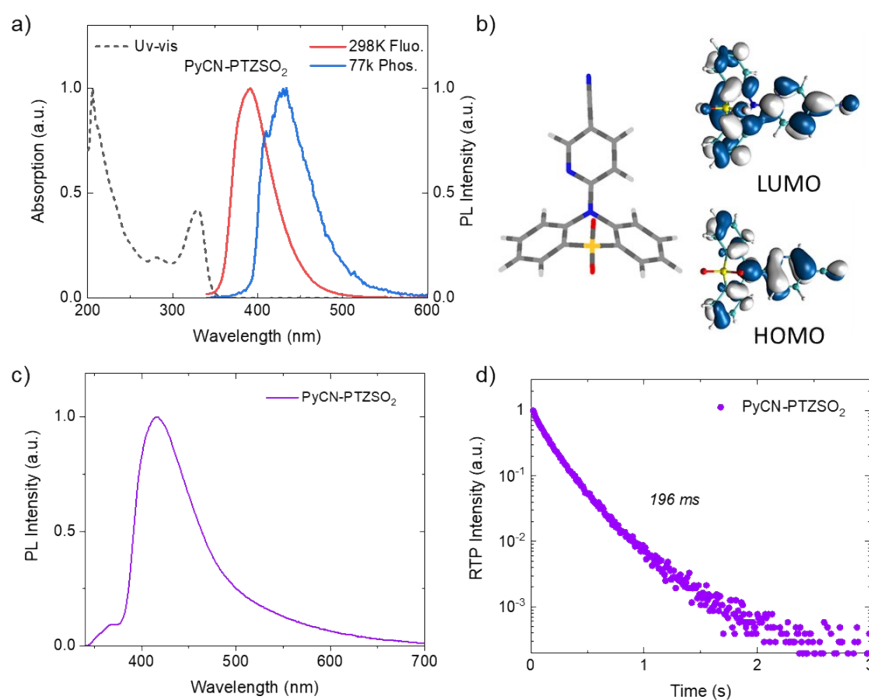


Fig. S16. a) Absorption, fluorescence and phosphorescence spectra of PyCN-PTZSO₂ in hexane solution (10⁻⁴ M). b) Optimized ground state structure and HOMO, LUMO distribution of PyCN-PTZSO₂ in M062x/TZVP level. c) PL spectrum and d) RTP decay curve (measured at 520nm) of PyCN-PTZSO₂ crystal.

According to the calculation results, PyCN-PTZSO₂ has a planar conformation in ground state. And the peaks of the absorption spectrum locate at the similar position as PyCN-PTZ but have different relative intensity, which indicates that the vertical transition has a transition-allowed π - π^* character. As a result of reduced ICT, the fluorescence profile has a LE feature with less red-shift, indicating that TICT does not happen in excited state. Moreover, in compared with PyCN-PTZ, the oxidation of sulfur atom diminishes the participation of lone pair electrons in transition, which partly contributes to the longer phosphorescence lifetime in single crystal. And this is in accordance with that reported by Tian et al.¹⁷ PyCN-PTZSO₂ crystal exhibits a redshift and broad emission, indicating that there are multiple intermolecular interactions in crystal. The red-shift emission in PL indicates the formation of molecular aggregates. And the aggregates in crystal state can suppress nonradiative transition of triplet excitons and induce electronic couplings, which prompt the ISC and reduce nonradiative transition to the same timescale as phosphorescence emission.^{18, 19} Overall, the phosphorescence in PyCN-PTZSO₂ with long lifetime can be attributed to 1) planar conformation with less spin mixing between singlet and triplet states, 2) reduced n- π^* transition character and 3) intermolecular interactions in aggregation state.

OLED fabrication: Indium-tin oxide (ITO) coated glass substrates were washed with ultrasonic sequentially in deionized water, acetone, and ethanol and treated with O₂ plasma for 2 min before fabrication. PEDOT: PSS (4083) was spin-coated onto the ITO substrate (3000 rpm) and annealed at 150 °C for 10 min for a 40 nm layer. PVK: poly-TPD (4: 1, m/m, 8 mg/mL in chlorobenzene, 3000 rpm) was spin-coated as a hole transporting and electron blocking layer onto the PEDOT: PSS layer and annealed at 125 °C for 10 min. Subsequently, an emission layer PyCN-PTZ (15 mg/mL in chlorobenzene, 3000 rpm) was spin-coated and annealed at 70 °C for 10 min to yield a 50 nm emission layer. The substrate was moved to an evaporation chamber, where DPEPO, TmPyPB, CsF, and Al were evaporated at evaporation rates of 0.6, 1, 0.1, and 3 Å s⁻¹, respectively, under a pressure of 8 × 10⁻⁵ Pa. The current density and luminance versus driving voltage characteristics and electroluminescence (EL) spectra were recorded by an optical analyzer, Photo Research PR745. EQE was calculated from the luminance, current density, and EL spectrum, assuming a Lambertian distribution. The size of the pixels is 0.1 cm².

Device structure: ITO/ PEDOT: PSS (40 nm)/ PVK: Poly-TPD (4:1, 30 nm)/ PyCN-PTZ (50 nm)/ DPEPO (10 nm)/ TmPyPB (45 nm)/ CsF (1 nm)/ Al

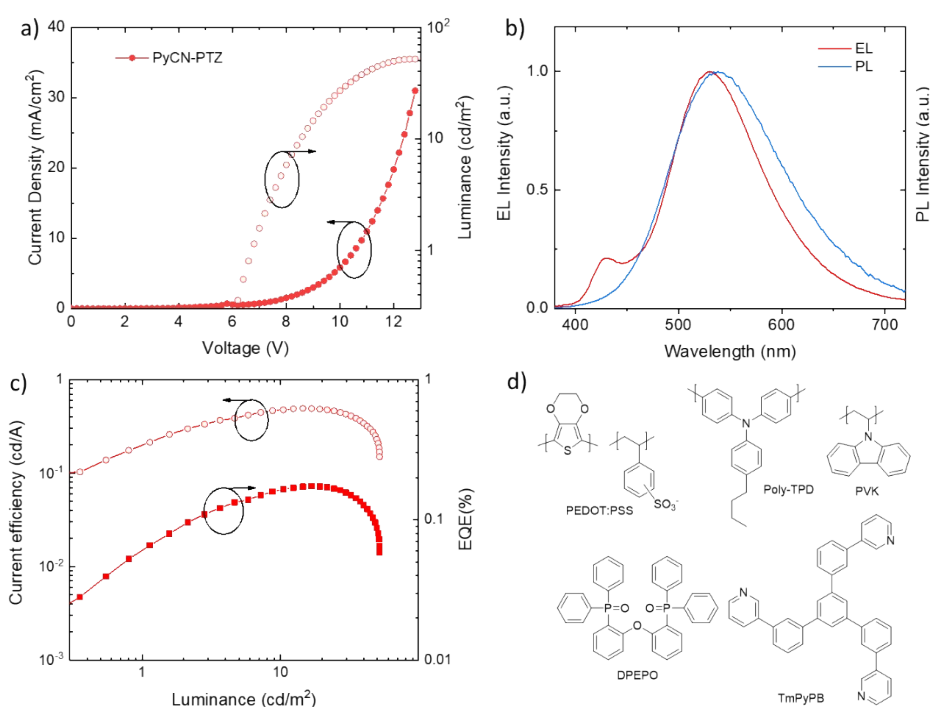


Fig. S17. a) Current density-voltage-luminance curves of OLED of PyCN-PTZ. b) Electroluminescence and PL spectrum of PyCN-PTZ. The spectra peak at the same wavelength, indicating that the emission form fluorescence and phosphorescence of PyCN-PTZ in TICT state. c) Current efficiency and external quantum efficiency (EQE) versus luminance curve of the OLED. d) Chemical structures of materials in OLED.

Table S9. Performance of solution process OLED based on PyCN-PTZ neat film including turn on voltage (V_{on}), maximum luminance (L_{max}), current efficiency (CE), power efficiency (PE) and maximum EQE (EQE_{max}) and CIE coordinate.

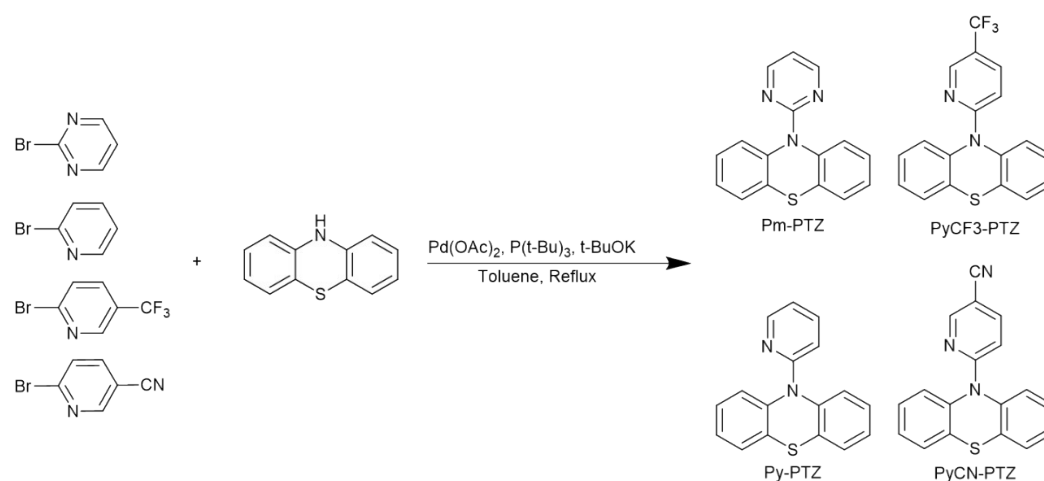
V_{on} (V)	L_{max} (cd/m ²)	CE (cd A ⁻¹)	PE (lm W ⁻¹)	EQE_{max} (%)	CIE (x,y)
6.8	51.89	0.49	0.17	0.17	(0.31, 0.49)

Table S10. Crystal information of the four compounds.

Name	Pm-PTZ	Py-PTZ	PyCF3-PTZ	PyCN-PTZ
Formula	C ₁₆ H ₁₁ N ₃ S	C ₁₇ H ₁₂ N ₂ S	C ₁₈ H ₁₁ F ₃ N ₂ S	C ₁₈ H ₁₁ N ₃ S
Space group	P 1	P 2 ₁ /n	P 1	P 2 ₁ /c
Cell length (Å)	a 7.8192(6) b 8.6756(5) c 10.6397(6)	a 8.12217(15) b 12.9649(2) c 12.5869(2)	a 8.2596(3) b 11.0005(6) c 16.8897(7)	a 8.7794(2) b 8.9521(3) c 18.1524(5)
Cell angles (°)	α 85.056(5) β 70.155(6) γ 68.937(6)	α 90 β 92.0384(15) γ 90	α 82.563(4) β 83.217(3) γ 77.214(4)	a 90 b 94.062(3) g 90
Cell Volume (Å ³)	633.008	1324.6	1477.59	1423.09
Z	2	4	2	4

3. Synthesis routes

All solvents and reactants were purchased from commercial source, and phenothiazine was recrystallized using chloroform and ethanol to ensure the purity. The final products were further purified by recrystallization using dichloromethane and methanol and vacuum sublimation at ca. 150°C using a sublimation tube at 10⁻¹ Pa. Detailed synthesis routes, procedures and characterization of products are as below:



Scheme S1. Synthesis routes for Pm-PTZ, Py-PTZ, PyCF3-PTZ and PyCN-PTZ

Synthesis of 10-(pyrimidin-2-yl)-10H-phenothiazine (Pm-PTZ)

2-bromopyrimidine (953 mg, 6 mmol), 10H-phenothiazine (1.2 g, 6 mmol) and potassium t-Butoxide (1.15 g, 12 mmol) were dissolved into 100 mL toluene in a 250 mL round-bottom three-neck flask. Under nitrogen atmosphere, Palladium (II) acetate (60 mg) and P(t-Bu)₃ (1 mL, 1M in toluene) were added into the system. After further degassing for 15min, the reaction mixture was heated to 110 °C, stirring overnight. After the system was cooled to room temperature, the solvent was removed in reduced pressure. The residues were extracted with dichloromethane, washed with water and dried over MgSO₄. Further purification using column chromatography with petroleum ether/dichloromethane in 4/1 (v/v) as eluents. Finally, 1.2 g Pm-PTZ white solid was obtained (yield: 73%). δ_{H} (500 MHz, Chloroform-*d*) 8.38 (2 H, d, *J* 4.7), 7.76 (2 H, dd, *J* 8.1, 1.3), 7.44 (2 H, dd, *J* 7.8, 1.5), 7.36 (2 H, td, *J* 7.8, 1.5), 7.21 (2 H, td, *J* 7.6, 1.3), 6.77 (1 H, t, *J* 4.8). δ_{C} (126 MHz, CDCl₃) 160.07, 157.78, 139.92, 133.36, 128.52, 128.02, 126.46, 126.09, 113.77. APCI-MS *m/z* Calcd for C₁₆H₁₁N₃S: 277.35; found: 278.3 ((M+1)+)

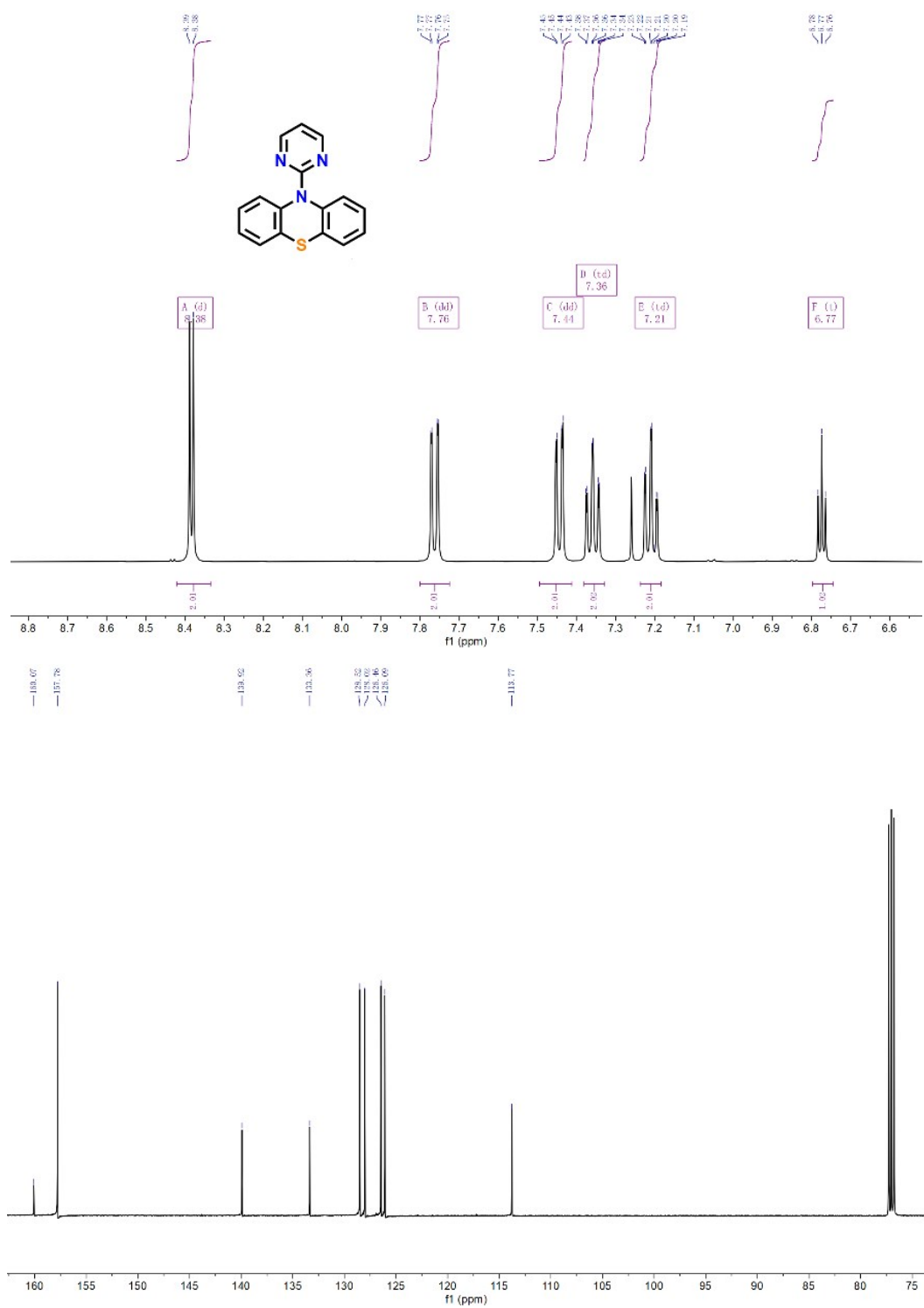


Fig. S18. ¹H NMR and ¹³C NMR of Pm-PTZ.

Synthesis of 10-(pyridin-2-yl)-10H-phenothiazine (Py-PTZ)

The synthesis of Py-PTZ followed the same procedure as Pm-PTZ, with 2-bromopyridine took the place of 2-bromopyrimidine. Finally, 1.36 g Py-PTZ white solid was obtained. (yield: 82%). δ_{H} (500 MHz, Chloroform-*d*) 8.30 (1 H, ddd, *J* 4.9, 2.1, 0.9), 7.58 (2 H, dd, *J* 8.1, 1.3), 7.48 (1 H, ddd, *J* 9.0, 7.3, 2.0), 7.39 (2 H, dd, *J* 7.8, 1.5), 7.29 (2 H, td, *J* 7.7, 1.5), 7.16 (2 H, dd, *J* 7.5, 1.3), 6.94 (1 H, dt, *J* 8.6, 1.0), 6.87

(1 H, ddd, J 7.2, 4.9, 0.9). δ_c (126 MHz, CDCl_3) 156.32, 148.00, 141.39, 137.73, 132.31, 128.08, 126.84, 126.43, 125.48, 116.99, 110.79, 77.26, 77.01, 76.76. APCI-MS m/z Calcd for $\text{C}_{17}\text{H}_{12}\text{N}_2\text{S}$: 276.07; found: 275.8.

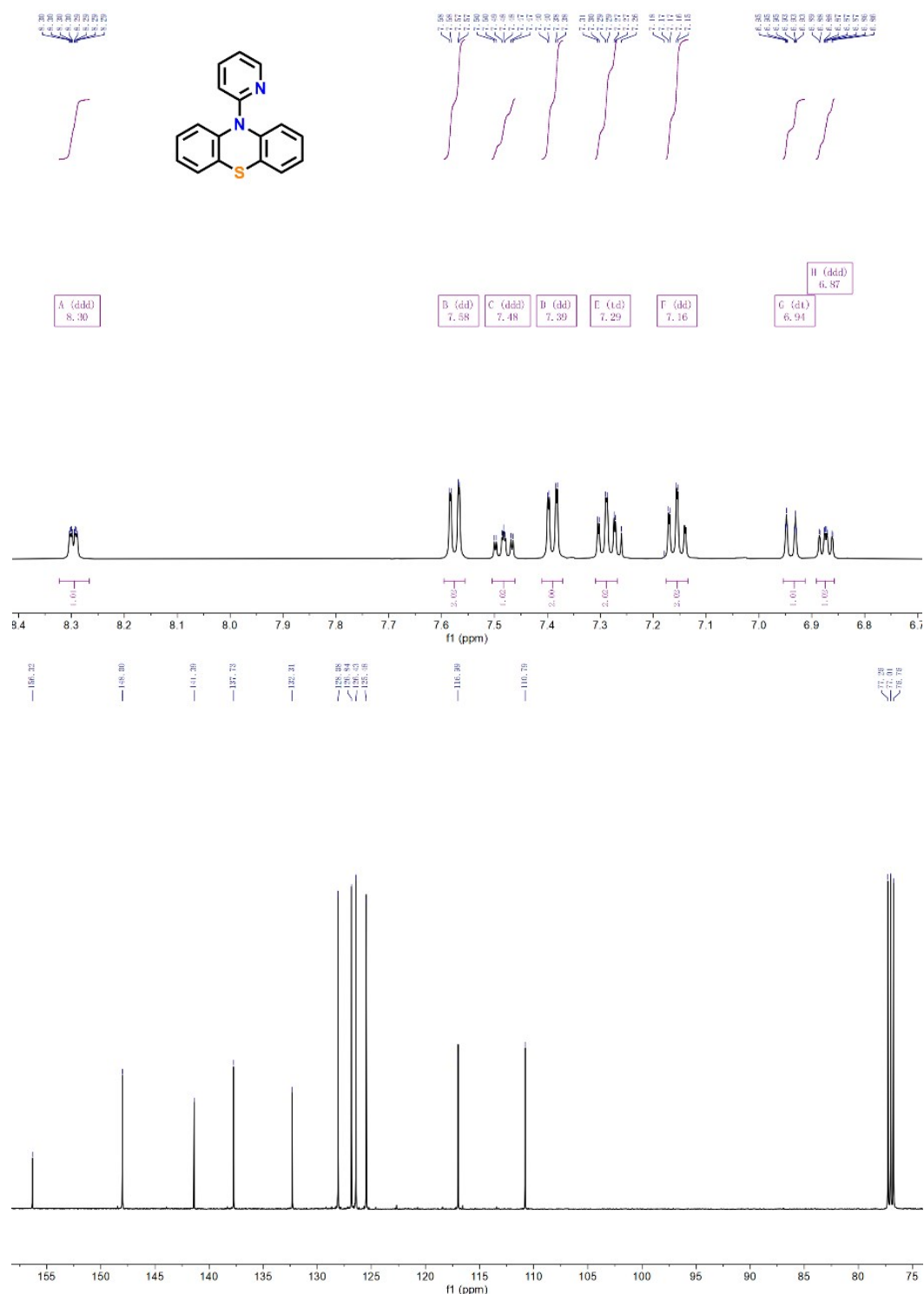


Fig. S19. ^1H NMR and ^{13}C NMR of Py-PTZ.

Synthesis of 10-(5-(trifluoromethyl)pyridin-2-yl)-10H-phenothiazine (PyCF3-PTZ)

The synthesis of PyCF3-PTZ followed the same procedure as Pm-PTZ, with 2-bromo-5-(trifluoromethyl)pyridine took the place of 2-bromopyrimidine. Finally, 1.28 g PyCF3-PTZ white solid was obtained.

(yield: 62.1%). δ_H (500 MHz, DMSO- d_6) 8.54 – 8.49 (1 H, m), 7.93 (1 H, dd, J 9.1, 2.6), 7.79 (2 H, dd, J 8.0, 1.3), 7.63 (2 H, dd, J 7.8, 1.5), 7.49 (2 H, td, J 7.7, 1.4), 7.37 (2 H, td, J 7.6, 1.3), 6.96 (1 H, d, J 9.0). δ_C (126 MHz, DMSO) 158.46, 145.72, 139.86, 135.85, 133.67, 128.93, 128.76, 127.94, 127.32, 125.90, 123.74, 107.68. APCI-MS m/z Calcd for $C_{18}H_{11}F_3N_2S$: 344.36; found: 343.7.

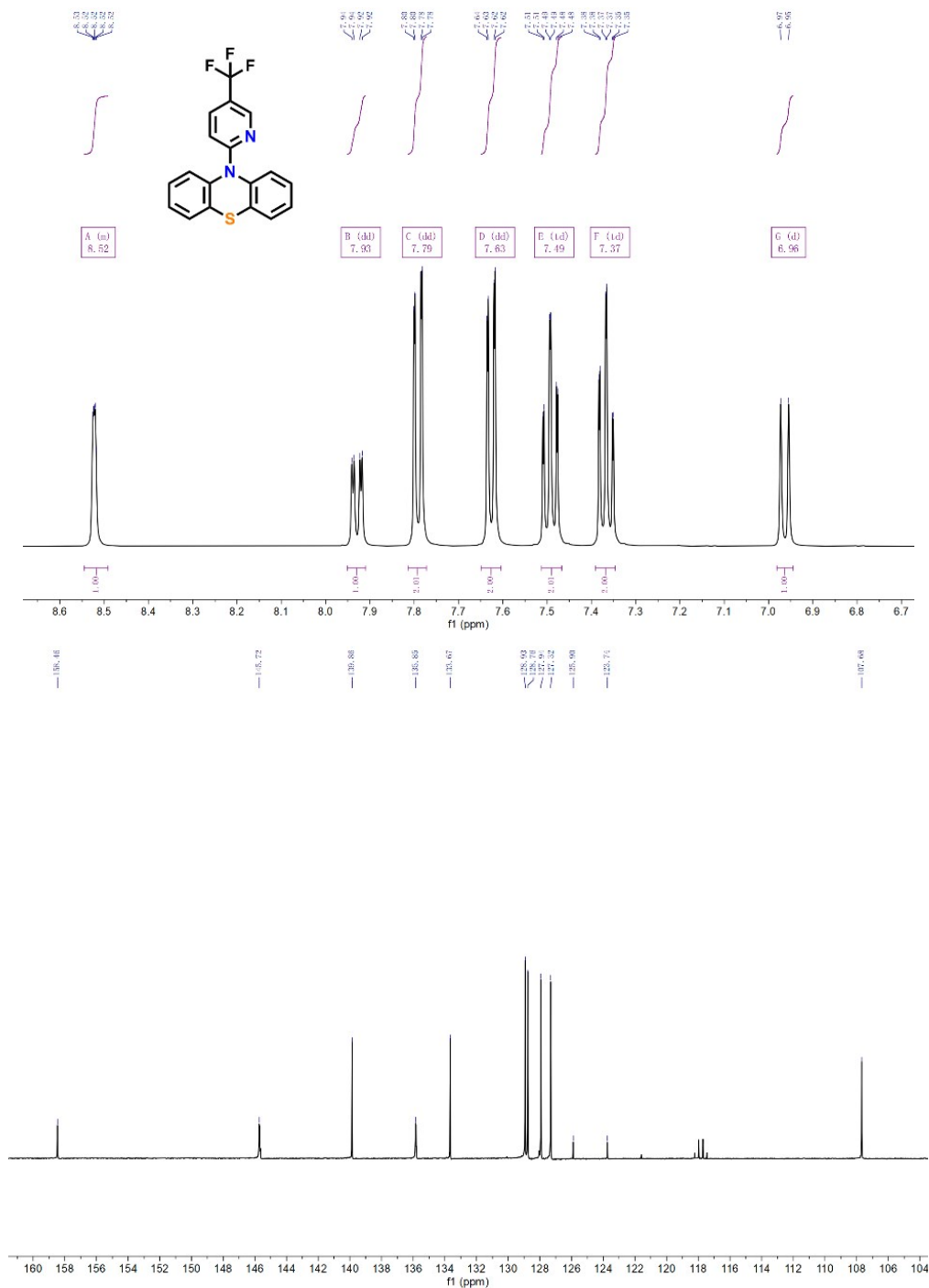


Fig. S20. 1H NMR and ^{13}C NMR of PyCF3-PTZ.

Synthesis of 6-(10H-phenothiazin-10-yl) nicotinonitrile (PyCN-PTZ)

The synthesis of PyCN-PTZ followed the same procedure as Pm-PTZ, with 6-bromonicotinonitrile

pyridine took the place of 2-bromopyrimidine. Finally, 1.3 g PyCN-PTZ white solid was obtained. (yield: 72.1%) δ_H (500 MHz, Chloroform-*d*) 8.44 (1 H, dd, *J* 2.3, 0.8), 7.67 (2 H, dd, *J* 8.0, 1.3), 7.59 (1 H, dd, *J* 9.0, 2.3), 7.49 (2 H, dd, *J* 7.8, 1.5), 7.39 (2 H, td, *J* 7.6, 1.5), 7.27 (2 H, dd, *J* 7.6, 1.4), 7.25 (1 H, d, *J* 1.3), 6.88 (1 H, dd, *J* 8.9, 0.8). δ_C (126 MHz, CDCl₃) 157.79, 152.29, 139.99, 139.31, 134.26, 128.64, 127.93, 127.07, 126.85, 117.93, 107.47, 100.42. APCI-MS *m/z* Calcd for C₁₈H₁₁N₃S: 301.37; found: 300.7

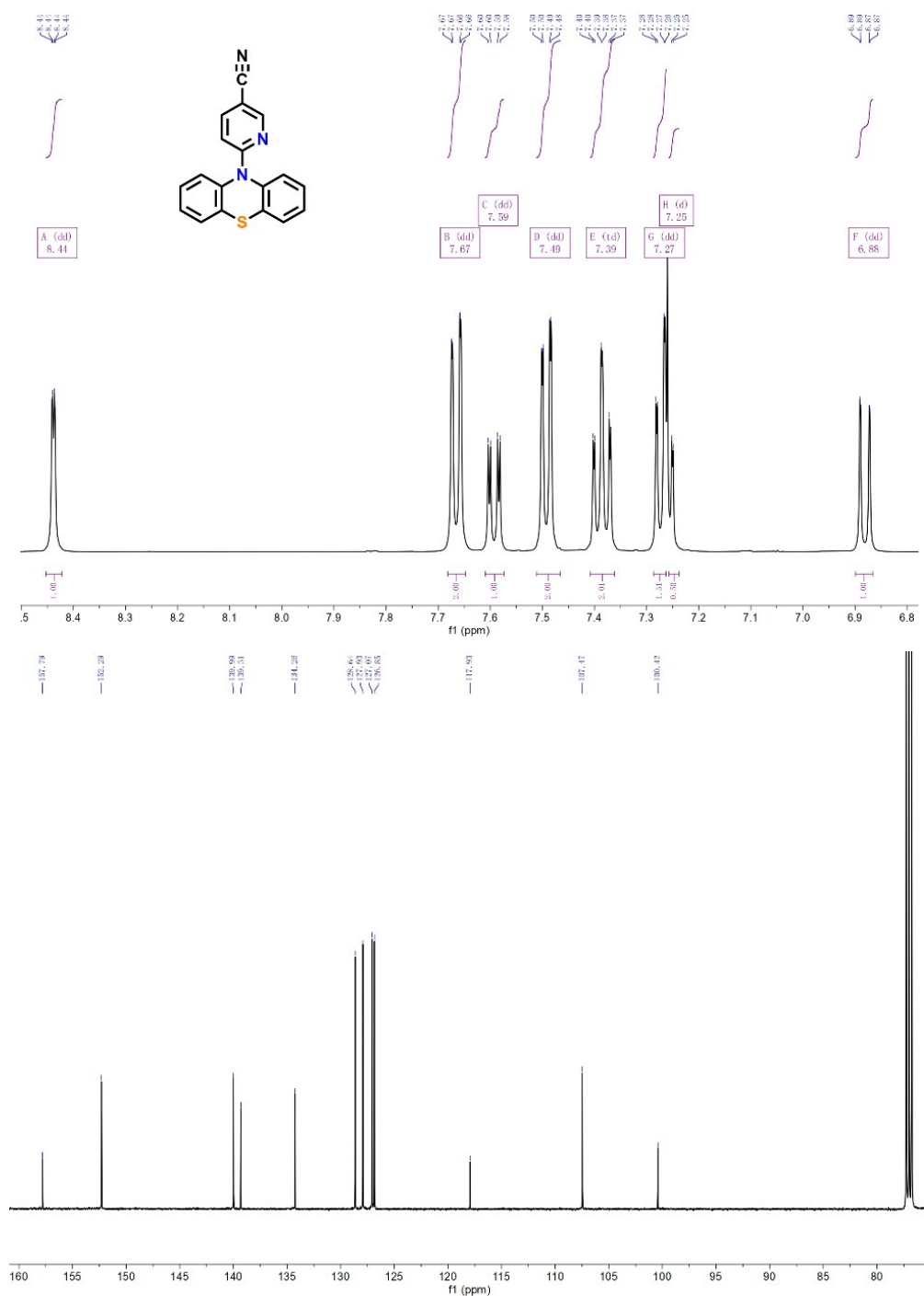
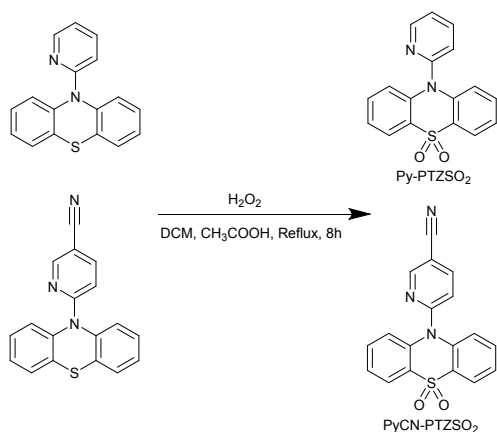


Fig. S21. ¹H NMR and ¹³C NMR of PyCN-PTZ.



Scheme S2. Synthesis routes for Py-PTZSO₂ and PyCN-PTZSO₂.

Synthesis of 10-(pyridin-2-yl)-10H-phenothiazine 5,5-dioxide (Py-PTZSO₂)

Py-PTZ (602 mg, 2mmol) was dissolved in dichloromethane (40 mL) and ethanoic acid (20 mL) in a 250 mL round-bottom flask. 5 mL H₂O₂ was added and reflux for 8h. After cooling to room temperature, the system was extracted with dichloromethane, washed with water and sodium bicarbonate solution and dried over MgSO₄. Further purification using column chromatography with petroleum ether/dichloromethane in 1/2 (v/v) as eluents and recrystallization with carbinol and dichloromethane to obtain 560 mg Py-PTZSO₂ as white solid (yield: 91%). ¹H NMR (500 MHz, Chloroform-d) δ 8.89 – 8.84 (m, 1H), 8.15 (dd, J = 7.9, 1.6 Hz, 2H), 8.04 (td, J = 7.7, 2.0 Hz, 1H), 7.56 (ddd, J = 7.5, 4.9, 1.1 Hz, 1H), 7.46 – 7.36 (m, 3H), 7.27 (td, J = 7.6, 7.2, 1.0 Hz, 2H), 6.65 (dd, J = 8.6, 1.0 Hz, 2H). ¹³C NMR (126 MHz, CDCl₃) δ 152.81, 150.99, 140.85, 140.48, 140.21, 132.78, 125.05, 124.67, 123.53, 123.35, 122.56, 117.27, 77.29, 77.24, 77.04, 76.78.

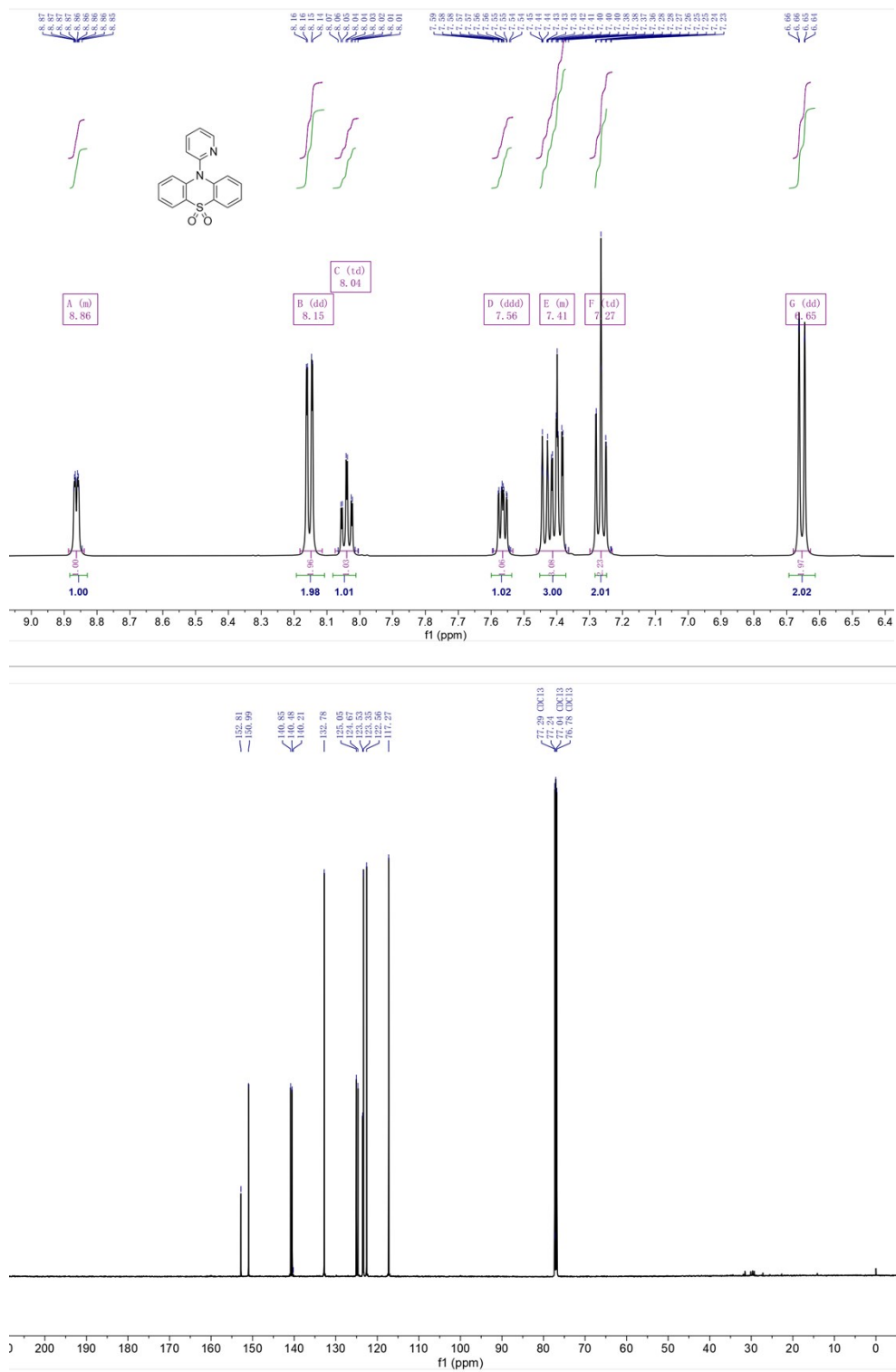


Fig. S22. ¹H NMR and ¹³C NMR of Py-PTZSO₂.

Synthesis of 6-(5,5-dioxido-10H-phenothiazin-10-yl)nicotinonitrile (PyCN-PTZSO₂)

The synthesis of PyCN-PTZSO₂ followed the same procedure as Py-PTZSO₂, with PyCN-PTZ took the place of Py-PTZ. Finally, 620 mg PyCN-PTZ white solid was obtained. (yield: 93%). ¹H NMR (500 MHz,

Chloroform-*d* δ 8.79 (dd, $J = 2.3, 0.8$ Hz, 1H), 8.10 (dd, $J = 7.9, 1.4$ Hz, 2H), 7.94 (dd, $J = 8.6, 2.3$ Hz, 1H), 7.64 – 7.52 (m, 4H), 7.44 (ddd, $J = 8.1, 6.5, 1.9$ Hz, 2H), 7.28 (dd, $J = 8.7, 0.8$ Hz, 1H). ^{13}C NMR (126 MHz, CDCl_3) δ 156.86, 152.44, 141.93, 140.49, 132.77, 131.07, 125.52, 123.94, 123.63, 116.80, 106.16, 53.44, 0.00.

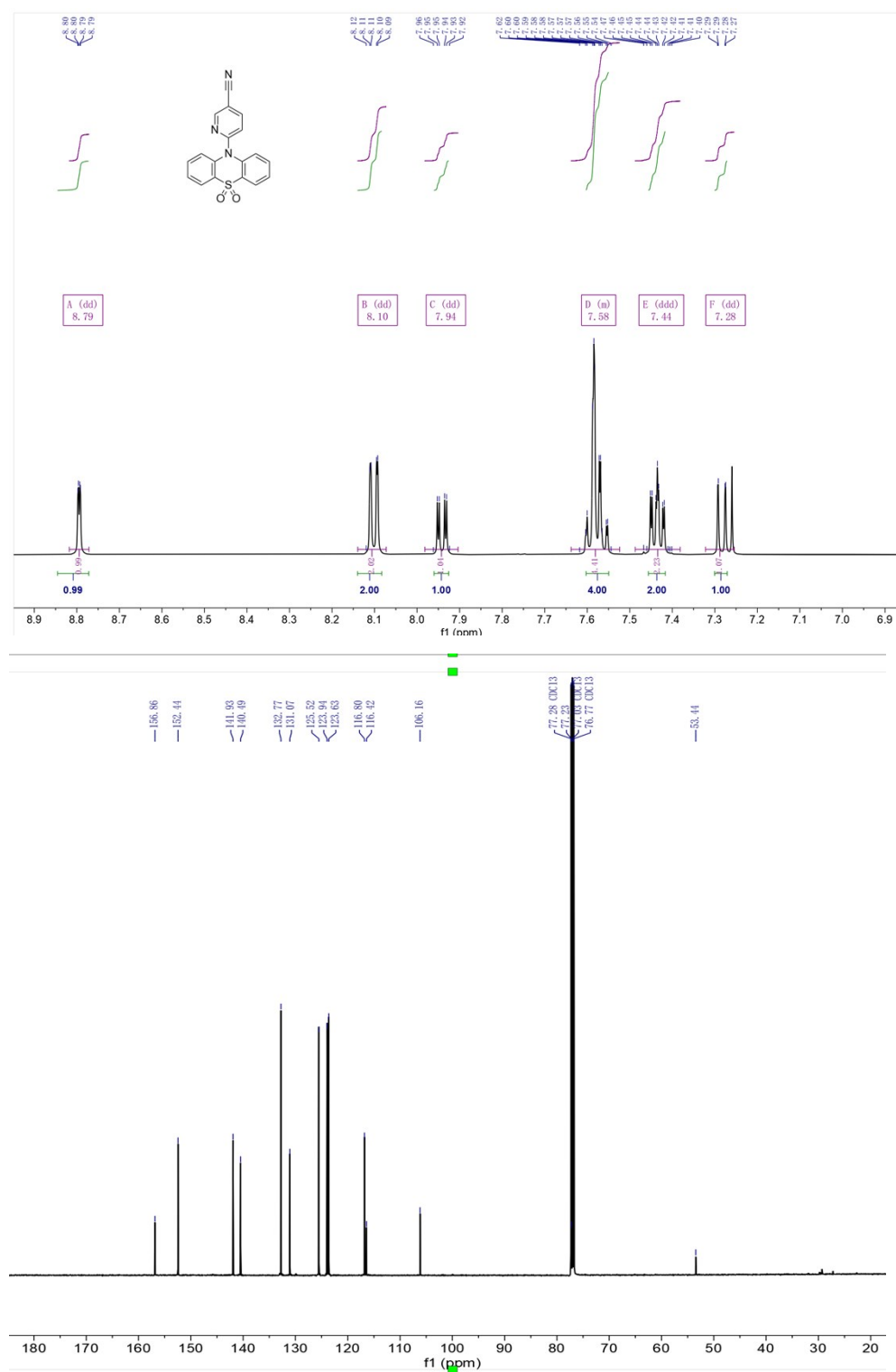


Fig. S23. ¹H NMR and ¹³C NMR of PyCN-PTZSO₂.

Reference

1. R. A. Gaussian 09, M. J. Frisch, G. W. Trucks, H. B. Schlegel, G. E. Scuseria, M. A. Robb, J. R. Cheeseman, G. Scalmani, V. Barone, G. A. Petersson, H. Nakatsuji, X. Li, M. Caricato, A. Marenich, J. Bloino, B. G. Janesko, R. Gomperts, B. Mennucci, H. P. Hratchian, J. V. Ortiz, A. F. Izmaylov, J. L. Sonnenberg, D. Williams-Young, F. Ding, F. Lipparini, F. Egidi, J. Goings, B. Peng, A. Petrone, T. Henderson, D. Ranasinghe, V. G. Zakrzewski, J. Gao, N. Rega, G. Zheng, W. Liang, M. Hada, M. Ehara, K. Toyota, R. Fukuda, J. Hasegawa, M. Ishida, T. Nakajima, Y. Honda, O. Kitao, H. Nakai, T. Vreven, K. Throssell, J. A. Montgomery, Jr., J. E. Peralta, F. Ogliaro, M. Bearpark, J. J. Heyd, E. Brothers, K. N. Kudin, V. N. Staroverov, T. Keith, R. Kobayashi, J. Normand, K. Raghavachari, A. Rendell, J. C. Burant, S. S. Iyengar, J. Tomasi, M. Cossi, J. M. Millam, M. Klene, C. Adamo, R. Cammi, J. W. Ochterski, R. L. Martin, K. Morokuma, O. Farkas, J. B. Foresman, and D. J. Fox, Gaussian, Inc., Wallingford CT, 2016.
2. E. Runge and E. K. U. Gross, *Phys. Rev. Lett.*, 1984, **52**, 997-1000.
3. A. Dreuw and M. Head-Gordon, *Chem. Rev.*, 2005, **105**, 4009-4037.
4. P. J. Stephens, F. J. Devlin, C. F. Chabalowski and M. J. Frisch, *J. Phys. Chem.*, 1994, **98**, 11623-11627.
5. Y. Zhao and D. G. Truhlar, *Theor. Chem. Acc.*, 2008, **120**, 215-241.
6. T. Lu and F. Chen, *J. Comput. Chem.*, 2012, **33**, 580-592.
7. W. Humphrey, A. Dalke and K. Schulten, *J. Mol. Graph.*, 1996, **14**, 33-38, 27-38.
8. X. Gao, S. Bai, D. Fazzi, T. Niehaus, M. Barbatti and W. Thiel, *J. Chem. Theory Comput.*, 2017, **13**, 515-524.
9. E. C. Lim, *Acc. Chem. Res.*, 2002, **20**, 8-17.
10. N. Nishimura, Z. Lin, K. Jinnai, R. Kabe and C. Adachi, *Adv. Funct. Mater.*, 2020, **30**, 2000795.
11. R. Kabe and C. Adachi, *Nature*, 2017, **550**, 384-387.
12. N. J. Turro, V. Ramamurthy and J. C. Scaiano, *Modern molecular photochemistry of organic molecules*, University Science Books, Sausalito, California, 2010.
13. K. Narushima, Y. Kiyota, T. Mori, S. Hirata and M. Vacha, *Adv. Mater.*, 2019, **31**, 1807268.
14. S. Hirata, *Adv. Sci.*, 2019, **6**, 1900410.
15. C. Deng, L. Zhang, D. Wang, T. Tsuboi and Q. Zhang, *Adv. Opt. Mater.*, 2019, **7**.
16. S. Hirata, *Adv. Opt. Mater.*, 2017, **5**, 1700116.
17. S. Tian, H. Ma, X. Wang, A. Lv, H. Shi, Y. Geng, J. Li, F. Liang, Z. M. Su, Z. An and W. Huang, *Angew. Chem. Int. Ed.*, 2019, **58**, 6645-6649.
18. S. Pan, Z. Chen, X. Zheng, D. Wu, G. Chen, J. Xu, H. Feng and Z. Qian, *J. Phys. Chem. Lett.*, 2018, **9**, 3939-3945.
19. J. Yang, X. Zhen, B. Wang, X. Gao, Z. Ren, J. Wang, Y. Xie, J. Li, Q. Peng, K. Pu and Z. Li, *Nat. Commun.*, 2018, **9**, 840.